Article

In vivo base editing rescues Hutchinson–Gilford progeria syndrome in mice

https://doi.org/10.1038/s41586-020-03086-7

Received: 9 June 2020

Accepted: 30 November 2020

Published online: 6 January 2021

Check for updates

Luke W. Koblan[1,2,3,13], Michael R. Erdos[4,13], Christopher Wilson[1,2,3], Wayne A. Cabral[4], Jonathan M. Levy[1,2,3], Zheng-Mei Xiong[4], Urraca L. Tavarez[4], Lindsay M. Davison[5], Yantenew G. Gete[6], Xiaojing Mao[6], Gregory A. Newby[1,2,3], Sean P. Doherty[5], Narisu Narisu[4], Quanhu Sheng[7], Chad Krilow[4], Charles Y. Lin[8,9,12], Leslie B. Gordon[10,11], Kan Cao[6], Francis S. Collins[4]✉, Jonathan D. Brown[5]✉ & David R. Liu[1,2,3]✉

Hutchinson–Gilford progeria syndrome (HGPS or progeria) is typically caused by a dominant-negative C•G-to-T•A mutation (c.1824 C>T; p.G608G) in *LMNA*, the gene that encodes nuclear lamin A. This mutation causes RNA mis-splicing that produces progerin, a toxic protein that induces rapid ageing and shortens the lifespan of children with progeria to approximately 14 years[1–4]. Adenine base editors (ABEs) convert targeted A•T base pairs to G•C base pairs with minimal by-products and without requiring double-strand DNA breaks or donor DNA templates[5,6]. Here we describe the use of an ABE to directly correct the pathogenic HGPS mutation in cultured fibroblasts derived from children with progeria and in a mouse model of HGPS. Lentiviral delivery of the ABE to fibroblasts from children with HGPS resulted in 87–91% correction of the pathogenic allele, mitigation of RNA mis-splicing, reduced levels of progerin and correction of nuclear abnormalities. Unbiased off-target DNA and RNA editing analysis did not detect off-target editing in treated patient-derived fibroblasts. In transgenic mice that are homozygous for the human *LMNA* c.1824 C>T allele, a single retro-orbital injection of adeno-associated virus 9 (AAV9) encoding the ABE resulted in substantial, durable correction of the pathogenic mutation (around 20–60% across various organs six months after injection), restoration of normal RNA splicing and reduction of progerin protein levels. In vivo base editing rescued the vascular pathology of the mice, preserving vascular smooth muscle cell counts and preventing adventitial fibrosis. A single injection of ABE-expressing AAV9 at postnatal day 14 improved vitality and greatly extended the median lifespan of the mice from 215 to 510 days. These findings demonstrate the potential of in vivo base editing as a possible treatment for HGPS and other genetic diseases by directly correcting their root cause.

Hutchinson–Gilford progeria syndrome (HGPS or progeria) is a rare genetic disease characterized by accelerated ageing[4]. In over 90% of patients with HGPS, the disease is caused by a single de novo point mutation (c.1824 C>T; p.G608G) in the lamin A (*LMNA*) gene[1,2]. This mutation potentiates a cryptic splice site in exon 11, leading to a mis-splicing event that results in the loss of 50 amino acids from the lamin A protein[1,2] (Fig. 1a). This truncated protein, which is known as progerin, lacks a proteolytic cleavage site for ZMPSTE24, which cleaves the farnesylated C terminus of wild-type pre-lamin A[1]. Progerin protein impairs nuclear structure and function, culminating in premature senescence and cell death[7]. The pathogenic mutation is dominant-negative, so a single copy of the allele is sufficient to cause progeria[3]. Cardiovascular disease—characterized by premature atherosclerosis, loss of vascular smooth muscle cells (VSMCs) and vascular stiffening—is the predominant cause of death in children with progeria, who have an average lifespan of approximately 14 years[3,7–11]. Although strategies for treating progeria, such as global inhibition of protein farnesylation[3,12,13], offer benefits to patients, no approach has yet been reported to directly reverse the mutation that causes HGPS[14–17].

The dominant-negative function of progerin poses challenges for the treatment of HGPS by gene augmentation or gene disruption strategies. Overexpression of wild-type *LMNA* does not rescue cellular phenotypes[18]. Although CRISPR–Cas9-mediated genetic disruption of the pathogenic allele has been reported to improve phenotypes in mouse models of progeria[15–17], the resulting diversity of uncharacterized

[1]Merkin Institute of Transformative Technologies in Healthcare, Broad Institute of Harvard and MIT, Cambridge, MA, USA. [2]Department of Chemistry and Chemical Biology, Harvard University, Cambridge, MA, USA. [3]Howard Hughes Medical Institute, Harvard University, Cambridge, MA, USA. [4]National Human Genome Research Institute, National Institutes of Health, Bethesda, MD, USA. [5]Division of Cardiovascular Medicine, Vanderbilt University Medical Center, Nashville, TN, USA. [6]Department of Cell Biology and Molecular Genetics, University of Maryland, College Park, MD, USA. [7]Department of Biostatistics, Vanderbilt University Medical Center, Nashville, TN, USA. [8]Department of Molecular and Human Genetics, Baylor College of Medicine, Houston, TX, USA. [9]Therapeutic Innovation Center, Department of Biochemistry and Molecular Biology, Baylor College of Medicine, Houston, TX, USA. [10]Hasbro Children's Hospital, Alpert Medical School of Brown University, Providence, RI, USA. [11]Boston Children's Hospital, Harvard Medical School, Boston, MA, USA. [12]Present address: Kronos Bio Inc., Cambridge, MA, USA. [13]These authors contributed equally: Luke W. Koblan, Michael R. Erdos. ✉e-mail: francis.collins3@nih.gov; jonathan.d.brown@vumc.org; drliu@fas.harvard.edu

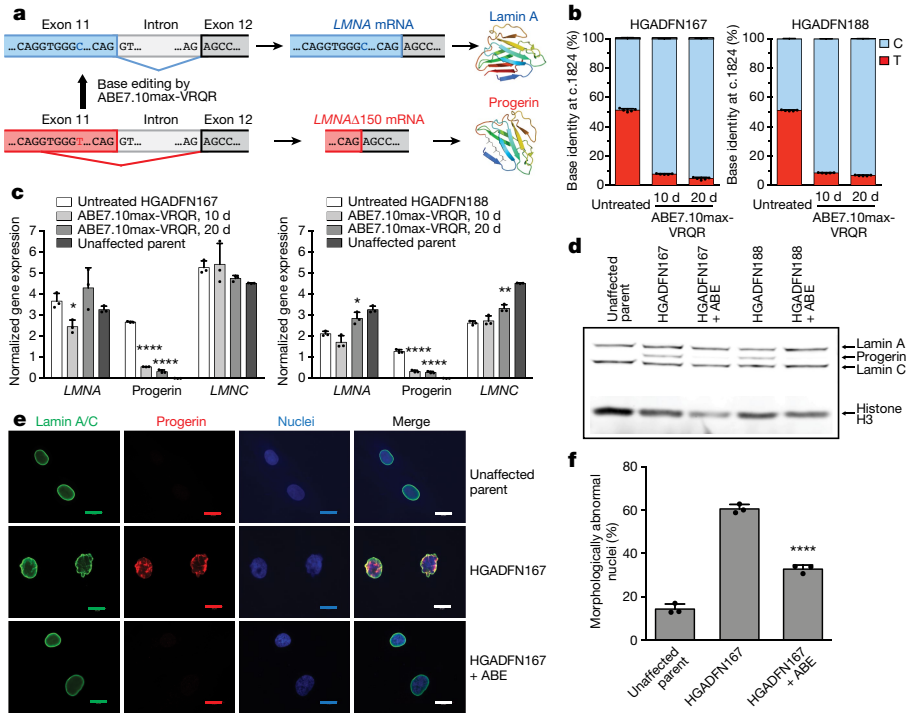

Fig. 1 | ABE-mediated correction of the *LMNA* c.1824 C>T mutation in fibroblasts derived from patients with progeria. a, The *LMNA* c.1824 C>T mutation potentiates a cryptic splice site in exon 11 of the *LMNA* gene, resulting in an in-frame deletion of 150 nt (*LMNA*Δ150) and production of the pathogenic progerin protein. **b**, *LMNA* c.1824 nucleotide identity in untreated patient-derived HGADFN167 and HGADFN188 cells and in cells 10 or 20 days after treatment with ABE7.10max-VRQR lentivirus. Data are mean ± s.d. of five technical replicates. **c**, Quantification by digital droplet PCR (ddPCR) of *LMNA*, progerin and *LMNC* (a normal alternative splice form) transcripts in untreated patient-derived cells, cells 10 or 20 days after treatment with ABE lentivirus and cells from an unaffected parent. Gene expression levels were normalized to transferrin receptor (*TFRC*) expression levels. Data from the unaffected parent are shown in both graphs for comparison. Data are mean ± s.d. of three technical replicates. **d**, Western blot of unaffected parent cells, untreated patient-derived cells or patient-derived cells 20 days after ABE lentiviral treatment using the JOL2 antibody specific for human lamin A, progerin and lamin C. Complete blots with molecular weight markers are available in Supplementary Fig. 1. Additional independent biological replicates are provided in Extended Data Fig. 1. **e**, Nuclear morphology of unaffected parent cells, untreated HGADFN167 cells or HGADFN167 cells 20 days after treatment with ABE-expressing lentivirus, stained with a lamin-A-specific antibody, a progerin-specific antibody or DAPI. Scale bars, 20 µm. Additional replicates were not performed. **f**, Frequency of morphologically abnormal nuclei in samples of cells shown in **e**. Data are mean ± s.d. from three counts of independent images from the experiment in **e**. *$P < 0.05$, **$P < 0.01$, ***$P < 0.001$, ****$P < 0.0001$ by Student's unpaired two-sided *t*-test.

insertion and deletion (indel) products at the target locus together with the risk of disrupting the wild-type *LMNA* allele, which differs only at a single base pair from the pathogenic allele[19,20], pose challenges to clinical translation of gene disruption strategies to treat progeria.

Base editors are genome editing agents that directly convert targeted base pairs without making double-strand DNA breaks[6]. Cytosine base editors (CBEs)[21] convert C•G to T•A, whereas adenine base editors (ABEs)[5] convert A•T to G•C. Base editors function in many mitotic and post-mitotic cell types and in a wide array of organisms[6]. ABEs use a laboratory-evolved deoxyadenosine deaminase to convert adenine to inosine (which base pairs like guanine) within a small window of around 4–5 nucleotides at a Cas-protein-specified locus, and induce the cell to replace the complementary thymine with cytosine by nicking and stimulating repair of the non-edited strand[5,6].

Here we report ABE-mediated correction of the *LMNA* c.1824 C>T mutation in fibroblasts derived from children with HGPS and in a mouse model in which mice contain two genomically integrated copies of the human *LMNA* c.1824 C>T progeria allele[22]. In cultured patient-derived cells, we observed efficient (around 90%) genomic DNA correction that ameliorates pathogenic mis-splicing of the *LMNA* transcript, reduces the abundance of progerin protein and restores normal nuclear morphology. When delivered into a mouse model of human progeria by single retro-orbital injection of therapeutically relevant doses of AAV9 encoding the ABE and single-guide RNA (sgRNA), the ABE corrected the *LMNA* c.1824 C>T allele in various tissues at the DNA, RNA and protein levels. Mice treated at postnatal day 14 (P14) showed a notable improvement in vascular disease compared to saline-injected controls, with aortic VSMC counts and adventitial fibrosis indistinguishable from those of wild-type mice, as well as reduced numbers of progerin-positive VSMCs and increased numbers of lamin A or lamin C (lamin A/C)-positive VSMCs. The median lifespan of ABE-treated mice with progeria was up to 2.4-fold longer than that of saline-injected controls. These findings suggest a potential therapeutic strategy for HGPS that directly corrects the causative mutation in vivo, and will inform applications of base editors in the treatment of other genetic diseases.

ABE corrects the HGPS mutation in patient cells

To position the pathogenic *LMNA* c.1824 C>T mutation within the activity window of an ABE[5] (positions 4–7, where the protospacer-adjacent motif (PAM) is positions 21–23), we chose a target site with an NGA PAM that places the mutation at protospacer position 6. To target this PAM, we used ABEmax-VRQR[23], which combines an optimized ABE7.10 variant[24] with an engineered SpCas9-VRQR variant[25] that targets NGA PAMs.

We tested the ability of ABEmax-VRQR to correct the mutation in two primary fibroblast cell lines derived from patients with progeria—HGADFN167 and HGADFN188 (Methods)—using a lentivirus to deliver ABEmax-VRQR and the sgRNA targeting the *LMNA* c.1824 C>T mutation. After lentiviral transduction and puromycin selection of HGADFN167 and HGADFN188 cells, we observed 84% and 85% correction of the pathogenic mutation

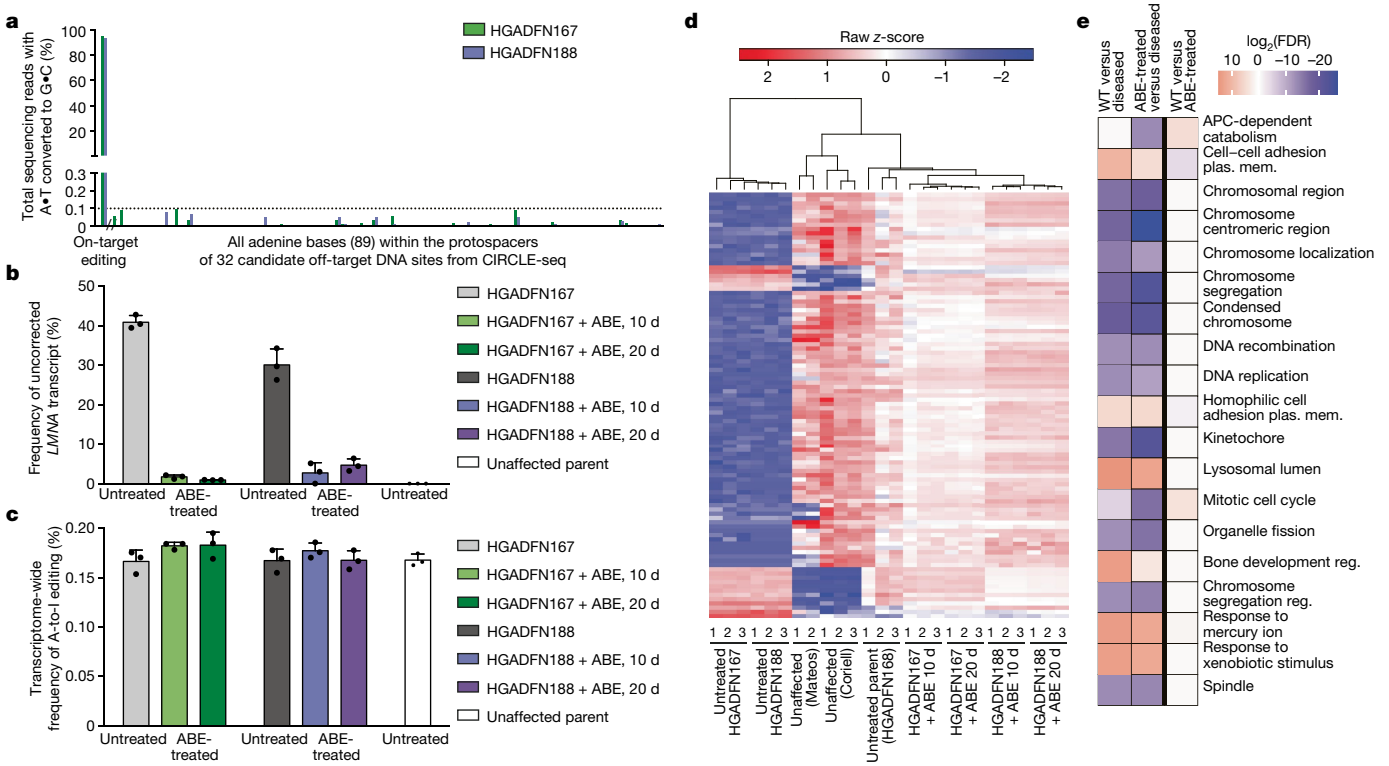

Fig. 2 | Analysis of off-target DNA and RNA editing and gene expression changes after treating fibroblasts derived from patients with progeria with ABEmax-VRQR. a, DNA sequencing for the top 32 CIRCLE-seq-identified[26] candidate off-target loci from HGADFN167 and HGADFN188 cells 20 days after treatment with ABE-expressing lentivirus. **b**, Uncorrected *LMNA* transcript frequency by RNA-seq in unaffected parental cells, untreated patient-derived cells and patient-derived cells 10 or 20 days after treatment with ABE-expressing lentivirus. Data are mean ± s.d. of three technical replicates. **c**, Transcriptome-wide cellular levels of A-to-I RNA editing in unaffected parental cells, untreated patient-derived cells and patient-derived cells 10 or 20 days after treatment with ABE-expressing lentivirus. Data are mean ± s.d. of three technical replicates. **d**, Heat map of *z*-scores for the top 100 differentially expressed genes between unaffected control fibroblasts (obtained from the Coriell Cell Bank (Coriell) and from a previously published dataset[47] (Mateos); Methods) and untreated or lentiviral-ABE-treated patient-derived cells. Expression *z*-scores across each gene are scaled so that mean expression = 0 and s.d. = 1. Samples and genes are ordered by hierarchical clustering. Patient-derived cells treated with lentiviral ABE for 10 and 20 days cluster with unaffected fibroblasts. **e**, Gene ontology molecular function analysis of differentially expressed genes. The 19 most significantly enriched gene sets in the Broad Institute molecular signatures database were identified between differentially expressed genes in wild-type (WT) cells (Mateos[47], Coriell and unaffected parent), diseased cells (untreated HGADFN167 and HGADFN188) and treated cells (lentiviral-ABE-treated HGADFN167 and HGADFN188 at 10 and 20 days). A heat map of $\log_2$-transformed FDR values for these 19 gene sets is shown, with overexpressed gene sets in red and underexpressed gene sets in blue. Plas. mem., plasma membrane; reg., regulation.

at 10 days, and 87% and 91% correction at 20 days, respectively (Fig. 1b). A low frequency (1.1–2.2%) of bystander editing was observed at the A•T at protospacer position 10, which results in V690A (Extended Data Fig. 1a). Indel frequencies were minimal (0.15% or lower) for both cell lines (Extended Data Fig. 1b). These results indicate that an ABE can efficiently correct the HGPS mutation to wild type with few editing by-products at the target locus.

Consistent with genomic correction of *LMNA* c.1824 C>T, we observed an 8.1-fold and a 4.4-fold reduction in the levels of mis-spliced *LMNA* mRNA in ABE-lentivirus-transduced HGADFN167 and HGADFN188 cells, respectively, 20 days after treatment, compared to untreated cells (Fig. 1c). ABE treatment also reduced the levels of progerin protein by 6.1- and 15-fold, respectively, relative to untreated cells, and modestly increased lamin A abundance (Fig. 1d). Nuclear morphology improved in ABE-treated cells, which had 1.8-fold fewer abnormal nuclei compared to untreated cells (Fig. 1e, f, Extended Data Fig. 1c–e). Together, these results show that base editing to correct the *LMNA* c.1824 C>T mutation in cells derived from patients with HGPS rescues the molecular and phenotypic consequences of the mutation.

Off-target editing analysis in patient cells

Canonical ABE7.10 editors can induce Cas-dependent off-target DNA editing and transient, low-level Cas-independent off-target RNA editing[6]. Cas-independent off-target DNA editing by ABE7.10 has been reported to be minimal or undetectable[6]. To identify candidate Cas-dependent off-target DNA editing sites associated with the sgRNA and Cas9-VRQR variant used to correct the HGPS mutation, we performed CIRCLE-seq[26] on genomic DNA from HGADFN167 and HGADFN188 cells treated in vitro with Cas9-VRQR nuclease and the *LMNA*-targeting sgRNA (Extended Data Fig. 2). We performed targeted sequencing of genomic DNA at the top 32 candidate off-target loci identified by CIRCLE-seq in HGADFN167 and HGADFN188 cells 20 days after ABE lentivirus transduction. We observed no detectable off-target DNA editing (0.1% or less) at the 32 tested candidate off-target loci in either cell line, despite 87–91% on-target editing (Fig. 2a).

To assess off-target RNA editing, we performed transcriptome-wide RNA sequencing (RNA-seq) on ABE-lentivirus-treated or untreated HGADFN167 and HGADFN188 cells, measuring the frequency of adenine-to-inosine RNA deamination, which naturally occurs throughout the transcriptome from endogenous cellular deaminases[27]. The on-target nucleotide within the *LMNA* transcript was efficiently (more than 80%) corrected from U to C in ABE-treated cells (Fig. 2b). The average frequency and distribution of A-to-I conversion in the transcriptome of ABE-treated cells were similar to those of untreated cells (Fig. 2c, Extended Data Fig. 1h). Notably, ABE treatment of cells derived from patients with HGPS restored the transcriptome to a state resembling

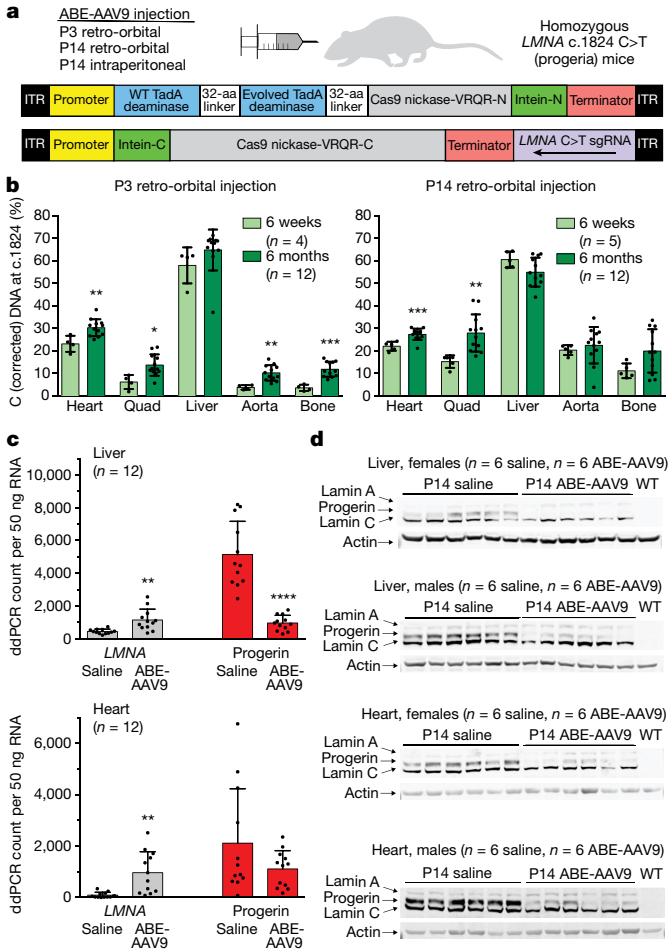

Fig. 3 | DNA, RNA and protein levels after a single in vivo injection of ABE-expressing AAV9 in a mouse model of human progeria. a, Dual AAV9 encoding split-intein ABE7.10max-VRQR base editor halves[28] and the *LMNA*-targeting sgRNA were injected into progeria mice. P3 retro-orbital injections (5×10^{10} vg of each AAV, 1×10^{11} vg total), P14 retro-orbital injections (5×10^{11} vg of each AAV, 1×10^{12} vg total) or P14 intraperitoneal injections (5×10^{11} vg of each AAV, 1×10^{12} vg total) were administered. ITR, inverted terminal repeats. **b**, DNA-editing efficiencies for correcting *LMNA* c.1824 from T (pathogenic) to C (wild type) in 6-week-old or 6-month-old mice that were retro-orbitally injected with ABE-expressing AAV9 (ABE-AAV9) at P3 (left) or P14 (right). Editing efficiencies in P14 intraperitoneally injected mice are shown in Extended Data Fig. 3a. **c**, ddPCR counts for the RNA transcript abundance of human *LMNA* (grey bars) and progerin (red bars) in the liver and heart of mice (6 months old) that were retro-orbitally injected with saline or ABE-AAV9 at P14. See Extended Data Fig. 4 for additional data. **d**, Western blot analysis of human lamin A, progerin and lamin C proteins in the liver and heart of mice that were retro-orbitally injected with saline or ABE-AAV9 at P14. Each lane shows tissue from a different mouse. 'WT' indicates a C57BL/6 mouse that lacks the transgene, showing that the antibody is specific to human lamin proteins. See Extended Data Fig. 5 for additional data. Data are mean ± s.d. for the indicated numbers of biological replicates. $^{*}P < 0.05$, $^{**}P < 0.01$, $^{***}P < 0.001$, $^{****}P < 0.0001$ by Student's unpaired two-sided *t*-test.

that of cells from an unaffected parent (Fig. 2d, e). These results collectively show that treating cells with the *LMNA*-targeting sgRNA and ABEmax-VRQR did not result in detected off-target DNA or RNA editing using the above analysis methods, despite high levels of on-target editing.

In vivo ABE delivery in mice with progeria

Encouraged by these findings, we applied base editing in vivo to correct a mouse model of progeria. We used C57BL/6 mice homozygous for a transgene that includes the complete human *LMNA* c.1824 C>T allele (C57BL/6-tg(LMNA*G608G)HCln/J, previously used as heterozygous mice[22]); these homozygous mice hereafter are referred to as 'progeria mice'. Phenotypically, this model recapitulates hallmark symptoms of HGPS including VSMC defects, hair loss, lack of subcutaneous fat, musculoskeletal abnormalities and shortened lifespan[3,4,22]. Given the diverse tissues affected by progeria, we sought systemic in vivo delivery of the ABE and sgRNA characterized above.

We recently developed a strategy for base editor delivery in vivo using adeno-associated virus (AAV)[28], a delivery modality that is approved by the US Food and Drug Administration (FDA). This approach uses *trans*-splicing inteins to reconstitute the full-length base editor in cells from a pair of AAVs, each expressing one half of the base editor[28,29] (Fig. 3a). We adapted this system to deliver ABEmax-VRQR and the *LMNA* c.1824-targeting sgRNA. We chose the AAV9 capsid for its broad tissue tropism, clinical validation and ability to transduce progeria-relevant tissues including heart and muscle[30,31].

To compare the effects of injection route and timing on in vivo editing, we performed retro-orbital injection of P3 (3-day-old) mice ($n = 4$) and P14 (2-week-old) mice ($n = 5$), and intraperitoneal injection of P14 mice ($n = 5$). P3 injections used 5×10^{10} viral genomes (vg) of each AAV for a total of 1×10^{11} vg per mouse. Both P14 injections used 5×10^{11} vg of each AAV for a total injection of 1×10^{12} vg per mouse. Mice were euthanized at the age of six weeks and editing was evaluated in various tissues (Fig. 3, Extended Data Fig. 3a–c).

At six weeks of age, P14 retro-orbital injection resulted in the highest editing efficiencies in aorta and bone among the tested injection routes (Fig. 3b, Extended Data Fig. 3a). Editing efficiencies in bulk heart tissue (excluding aorta) were similar for the three injection routes. P14 injections generally achieved higher base-editing efficiencies than P3 injections, possibly owing to the tenfold higher dose of AAV that could be injected into P14 mice or increased expression of AAV9 receptors in the older mice[28,32,33]. Together, these data reveal that a single in vivo injection of ABE-encoding AAV results in modest to high levels of correction (10–60%) of the causative *LMNA* point mutation in various organs.

Long-term ABE treatment of progeria mice

We performed long-term studies in mice using both P3 and P14 retro-orbital AAV injections to assess the relationship between long-term in vivo outcomes and editing efficiencies in disease-relevant tissues such as the aorta, in which editing levels in P14-injected mice were 3.8-fold higher relative to P3-injected mice at six weeks of age. We retro-orbitally injected 24 progeria mice at P3 with 10^{11} total vg of dual AAV9, and 24 mice at P14 with 10^{12} total vg as before. As controls, 24 mice at P3 and 24 mice at P14 were injected retro-orbitally with saline. All groups contained equal numbers of male and female mice. At 6 months of age, when untreated progeria mice typically show phenotypic decline but are not yet at the end of their lifespan, 24 P3-injected mice and 24 P14-injected mice (half AAV9-treated, half saline controls) were euthanized and analysed for DNA base-editing efficiency, *LMNA* RNA splicing, levels of human progerin and lamin proteins, and tissue histology. We placed the remaining 24 P3-injected mice and 24 P14-injected mice (half AAV9-treated, half saline controls) in a longevity study to assess lifespan.

DNA, RNA and protein analysis at six months

Analysis of the DNA base-editing outcomes in six-month-old mice revealed notable differences between the P3- and P14-injected cohorts. Both cohorts showed increases in DNA-editing efficiency in several tissues compared to the six-week time point (Fig. 3b). For example, editing in the aorta rose from 4.5 ± 2.5% to 10 ± 3.4% in P3-injected mice, and from 17 ± 5.2% to 23 ± 8.1% in P14-treated mice. Modest editing was observed in the lung, skin, visceral fat and white adipose tissue (WAT),

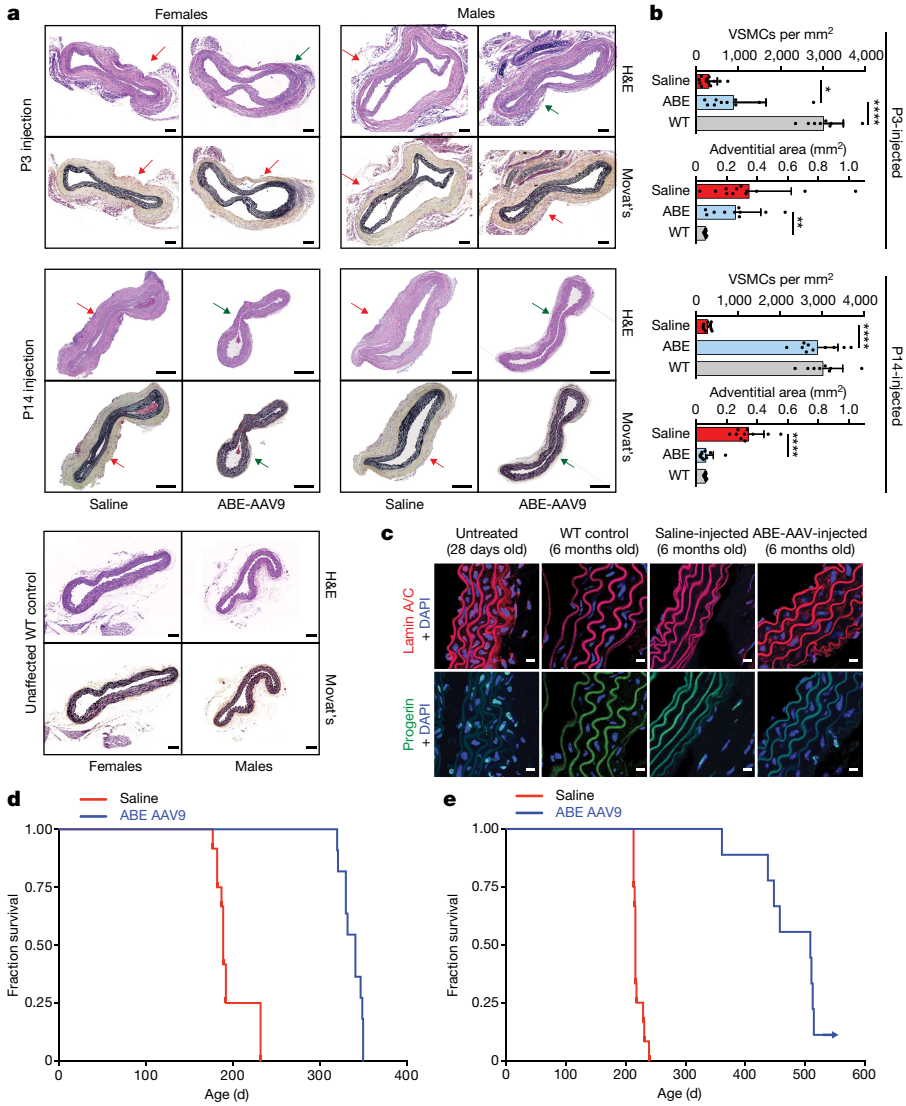

Fig. 4 | Aortic histopathology and lifespan of progeria mice after a single injection of ABE-AAV9. **a**, Representative aorta cross-sections from six-month-old mice showing VSMC nuclei and adventitia in mice that were retro-orbitally injected with saline or ABE-AAV9 at P3 or P14. Top images were stained with haematoxylin and eosin (H&E); bottom images were stained with Movat's pentachrome. Red arrows indicate decreased VSMC counts and adventitial fibrosis; green arrows indicate preserved VSMC counts and reduced adventitial fibrosis after AAV9-ABE treatment. Scale bars, 100 µm (P3 and wild type); 200 µm (P14). Additional replicates are shown in Extended Data Figs. 6, 7. **b**, Quantification of VSMC nuclei counts and adventitial area in mouse cohorts. Data are mean ± s.d. of $n = 12$ (P3 saline), $n = 10$ (P3 ABE-AAV9, P14 saline and P14 ABE-AAV9) or $n = 8$ (wild type) replicates. Data from wild-type samples are shown in both graphs for ease of comparison. Replicates analysed are provided in Extended Data Figs. 6, 7. **c**, Representative fixed aortas stained for human lamin A/C + DAPI and progerin + DAPI for untreated progeria mice at P28 (far left), wild-type C57BL/6 mice at 6 months (middle left), saline-injected progeria mice at 6 months (middle right) and ABE-treated progeria mice at 6 months (far right). Autofluorescent elastin fibres in the tunica media appear as wavy lines. Scale bars, 10 µm. Additional replicates are shown in Extended Data Fig. 8. **d**, Kaplan–Meier curve for mice that were retro-orbitally injected with saline ($n = 12$) or ABE-AAV9 ($n = 11$) at P3. Median lifespans: saline-injected mice, 189 days; ABE-AAV9-injected mice, 337 days (1.8-fold longer, $P < 0.0001$). **e**, Kaplan–Meier curve for mice that were retro-orbitally injected with saline ($n = 12$) or ABE-AAV9 ($n = 10$) at P14. Median lifespans: saline-injected mice, 215 days; ABE-AAV9-injected mice, 510 days (2.4-fold longer, $P < 0.0001$). *$P < 0.05$, **$P < 0.01$, ***$P < 0.001$, ****$P < 0.0001$ by Student's unpaired two-sided t-test (**b**) or Mantel–Cox test (**d**, **e**).

whereas editing was minimal in the kidney and spleen (Extended Data Fig. 3d). Bystander V690A editing and indels varied by tissue but were generally observed at low frequencies compared to on-target editing (Extended Data Fig. 3e, f). These results suggest that base editing may continue in vivo from six weeks to six months of age, consistent with the known persistence of AAV in mammals[34,35], or that edited cells may have a survival advantage over uncorrected cells in some organs, increasing the prevalence of edited alleles over time.

Editing efficiencies at six months in most tissues remained higher in the P14-injected cohort than the P3-injected cohort, including by 2.2-fold in the aorta, 2.1-fold in skeletal muscle, 1.7-fold in bone and 1.4-fold in lung (Extended Data Fig. 3d). These results indicate that injecting mice with 10^{12} total vg at P14 results in higher levels of *LMNA* correction 6 months after treatment, compared to injecting mice with 10^{11} total vg at P3.

Next, we quantified the effects of in vivo ABE treatment on transcript abundance and protein levels for progerin and human lamin A in six-month-old mice. Base editing led to decreases in progerin transcript abundance (Fig. 3c, Extended Data Fig. 4) that were sometimes larger than DNA correction levels; for example, in P14 WAT we observed a 31% reduction in the levels of progerin mRNA despite only 4.0 ± 3.6% DNA correction. These findings suggest that corrected cells may be more transcriptionally active than uncorrected cells or that cells with higher transcriptional activity may be more efficiently edited in vivo. Finally, we noted increases in the abundance of correctly spliced *LMNA* transcripts among ABE-treated mice in a variety of tissues compared with saline-injected controls (Extended Data Fig. 4).

We evaluated the protein levels of progerin and lamin A in six-month-old mice by western blot. P14 ABE-treated mice showed robust reductions of progerin protein in the liver (87 ± 14% reduction), heart excluding aorta (86 ± 9.1% reduction) and aorta (49 ± 19% reduction) compared to saline-injected controls (Fig. 3d, Extended Data Fig. 5). P3 ABE-treated mice showed similar reductions in progerin levels (Extended Data Fig. 5). Levels of progerin protein were generally reduced more than those of progerin mRNA in the same organ, suggesting that corrected cells may be translationally more active than uncorrected cells. Together, these findings indicate that in vivo ABE-mediated correction of the pathogenic human *LMNA* c.1824 C>T allele in mice can reduce progerin RNA and protein levels in several clinically relevant tissues.

ABE treatment improves vascular pathology

To assess the physiological consequences of base editing the pathogenic *LMNA* c.1824 C>T allele, we performed histological analysis of aorta and adipose tissue. Patients with progeria exhibit a loss of VSMCs in aortic vessel walls and periadventitial thickening, which together contribute to aortic stiffening and the impairment of cardiac function[7–11]. We observed these hallmark vascular features of progeria

in saline-injected control mice[22] (Fig. 4a). Aortas from P3-injected ABE-treated mice at 6 months of age showed 3.3-fold higher average VSMC counts per cross-sectional area compared with saline-injected controls, but similar (1.2-fold lower) adventitial thickness (Fig. 4a, b, Extended Data Figs. 6, 7). Notably, P14 injection of ABE completely rescued both aortic VSMC counts (11-fold increase) and adventitial thickness (5.5-fold decrease) compared to saline-injected controls, such that P14 ABE-treated mice were indistinguishable from wild-type mice in these two parameters (Fig. 4a, b, Extended Data Figs. 6, 7).

Progerin-induced VSMC death is a key driver of mortality in patients with progeria[7,11]. The improvements in aortic pathology in ABE-treated mice prompted us to examine the protein levels of human progerin and lamin A/C in aortic VSMCs. Sections of aorta from saline- and P14 ABE-treated mice were fixed and stained with antibodies specific to human lamin A/C and human progerin (Fig. 4c, Extended Data Fig. 8). As expected given their young age, VSMC nuclei from four-week-old progeria mice stained robustly for both proteins (Fig. 4c, far left). No staining for human lamin A/C or progerin was observed in wild-type C57BL/6 aortic VSMCs, demonstrating antibody specificity (Fig. 4c, middle left). Consistent with VSMC counts, aortas from six-month-old saline-injected progeria mice contained virtually no VSMCs (Fig. 4c, middle right). By contrast, ABE-treated progeria mice maintained much higher numbers of VSMCs that expressed human lamin A/C, with minimal progerin (Fig. 4c, far right). These observations suggest that DNA base editing of around 25% in the aorta rescues two key vascular defects of progeria—VSMC loss and periadventitial fibrosis—while preserving the expression of lamin A/C and reducing the abundance of progerin in VSMCs.

Lipodystrophy (reduced subcutaneous body fat) is a clinical feature of patients with progeria[4]. ABE treatment modestly rescued the loss of the hypodermal fat layer in both P3- and P14-injected mice relative to saline-injected controls (Extended Data Figs. 9, 10). Both ABE-treated and saline-injected mice exhibited moderate dermal hypoplasia compared to wild-type C57BL/6 mice (Extended Data Figs. 9, 10).

ABE treatment extends progeria mouse lifespan

We conducted longevity studies on 24 P3-injected and 24 P14-injected progeria mice (half ABE-injected, half saline-injected, equal numbers of both sexes). Over the 1.5-year duration of the longevity studies, 3 of 48 mice were excluded after health issues that were deemed to be unrelated to progeria or treatment (Supplementary Note 1).

Body weights were maintained in both ABE-treated cohorts (Extended Data Fig. 11). The median survival of P3 saline-injected mice ($n = 12$) was 189 days, whereas that of P3 ABE-treated mice ($n = 11$) was 337 days (1.8-fold longer, $P < 0.0001$ by Mantel–Cox test) (Fig. 4d). The median survival of P14 saline-injected mice ($n = 12$) was 215 days, whereas that of P14 ABE-treated mice ($n = 10$) was 510 days (2.4-fold longer, $P < 0.0001$ by Mantel–Cox test) (Fig. 4e), which corresponds approximately to the beginning of old age in wild-type C57BL/6 mice[36]. P14-injected mice exhibited normal behaviour and vitality at ages well beyond the lifespan of saline-injected mice (Supplementary Videos 1–5). One of the P14 ABE-treated mice remains in apparent good health at the time of writing. Complete data from the mouse longevity study are in Supplementary Table 1.

Among the nine deceased P14-injected ABE-treated mice, necropsy revealed gastrointestinal necrosis in one, liver tumours in five and no apparent abnormalities in three (Supplementary Table 1). To investigate the potential origins of the liver tumours, we performed whole-genome sequencing of liver tissue from two P14 saline-injected mice and of livers and liver tumours from three P14 ABE-treated mice that showed liver tumours. Samples from all of the AAV-injected mice, but none from saline-injected mice, showed evidence of rare AAV integration in genomic regions where AAV integration has been previously associated with liver tumours in mice (*Abr*, *Alb*, *Focad* and *Ksr1*)[37] (Supplementary Data 1). Although samples from liver tumours showed similar numbers of AAV integration events as samples from non-tumour liver tissue, previous observations of AAV integration at these regions in liver tumours from AAV-injected mice[37] suggest that AAV integration may have contributed to liver tumour formation. We note that AAV-associated liver tumours, although documented in mice, have thus far not been reported in humans treated with therapeutic AAV vectors[38].

The fraction of A•T-to-G•C point mutations among all point mutations detected by whole-genome sequencing was not significantly different among saline-injected mouse liver tissue, ABE-treated mouse liver tissue and ABE-treated mouse tumour tissue (false discovery rate (FDR)-adjusted $P = 0.28–0.50$), suggesting that ABE treatment had no apparent effect on the relative genome-wide abundance of A•T-to-G•C point mutations (Extended Data Fig. 12a, b, Supplementary Data 2). We also searched for A•T-to-G•C mutations and indels in the exons, introns and regulatory regions defined by assay for transposase-accessible chromatin using sequencing (ATAC-seq) within 100 kb of 84 genes recurrently mutated in liver cancer (Methods), and found no evident patterns distinguishing saline-injected mouse liver tissue, ABE-treated mouse liver tissue or ABE-treated mouse tumour tissue (Extended Data Fig. 12c, Supplementary Data 3). These data collectively suggest no apparent role of base editing in liver tumour formation. Finally, we note that the progeria mice in this study contain two copies of human *RAB25* downstream of *LMNA*, and *RAB25* overexpression promotes human hepatocellular carcinoma[39], raising the possibility that expression of transgenic *RAB25* in these mice (confirmed in Extended Data Fig. 12d) may contribute to liver tumorigenesis that manifests only once lifespan is greatly extended. Additional studies are needed to understand the potential roles of uncorrected *LMNA* c.1824 C>T alleles, *RAB25*, AAV transduction, ABE treatment and mouse age in the long-term health of these mice.

Discussion

Correcting pathogenic alleles that cause devastating diseases is a long-standing challenge in medicine. Base editing provides an opportunity to directly correct point mutations that drive many disorders without requiring double-strand DNA breaks. Here we demonstrate direct correction of the mutation that underlies most HGPS cases using an ABE. In patient-derived cells, base editing efficiently corrects the pathogenic allele, substantially reduces RNA mis-splicing, decreases the abundance of progerin protein and rescues nuclear morphology abnormalities. Characterization of off-target DNA and RNA editing suggests a low degree of off-target editing in patient-derived cells, despite on-target editing of 87–91%.

Systemic injection of a single dose of dual AAV9 encoding the ABE and sgRNA into a mouse model of human progeria resulted in durable correction of the pathogenic allele, amelioration of RNA mis-splicing, reduction of progerin protein in various tissues and greatly improved aortic health, fully rescuing VSMC counts and adventitial fibrosis in progeria mice treated with ABE at P14, which in the course of normal mouse maturation corresponds to approximately year 5–6 in humans[36]. These findings are particularly encouraging because arterial pathology is a major determinant of morbidity and mortality in children with progeria[4,7,8].

These results also establish that single injections of an ABE packaged in a clinically relevant AAV capsid can greatly extend the lifespan of an animal model of progeria, with median lifespan increasing in P14-treated mice from 215 to 510 days—approaching old age in healthy C57BL/6 mice[36]. The marked improvements in aortic pathology, lifespan and vitality among P14-injected mice long after a single ABE treatment collectively suggest that this strategy has the potential to improve tissue function and lifespan in patients with progeria.

Although single administration with possible transient immunosuppression may help to mitigate potential immunological responses to

editing agents, efforts to translate these findings into patients must closely monitor immune responses to treatment. AAV integration and liver tumours observed in some of the longest-lived mice—consistent with previous reports of AAV-integration-induced liver tumours in mice[37,40–43]—further highlights the importance of vector and dose optimization as well as post-treatment monitoring, even though liver tumours have not yet been observed in humans treated with AAV vectors[38].

In some tissues, modest DNA editing resulted in disproportionately large benefits at the RNA, protein or tissue levels. For example, editing of around 25% in the aorta of P14-injected mice resulted in 11-fold higher VSMC counts, a 5-fold decrease in adventitia fibrosis and a lack of observed progerin-positive VSMC nuclei. The outsized benefits of DNA editing suggest that edited cells may contribute disproportionately to the health of tissues in this animal model. Further studies are needed to understand the molecular basis of this phenomenon.

A number of additional studies may further advance base-editing treatments for progeria towards clinical application. We recently reported ABE variants with much higher editing activity than ABE7.10max[44,45]. These variants could further increase editing efficiency and phenotypic rescue, or might reduce the required dosage. The timing of treatment may also need to be further optimized for best outcomes, taking into account the time to diagnosis. Finally, ABE editing has the potential to synergize with emerging progeria treatments[3,14–16] including farnesyltransferase inhibitors[3], other small-molecule drugs[14] or antisense oligonucleotides that target the mutant *LMNA* allele[18,46].

Online content

Any methods, additional references, Nature Research reporting summaries, source data, extended data, supplementary information, acknowledgements, peer review information; details of author contributions and competing interests; and statements of data and code availability are available at https://doi.org/10.1038/s41586-020-03086-7.

1. Eriksson, M. et al. Recurrent de novo point mutations in lamin A cause Hutchinson–Gilford progeria syndrome. *Nature* **423**, 293–298 (2003).
2. De Sandre-Giovannoli, A. et al. Lamin A truncation in Hutchinson–Gilford progeria. *Science* **300**, 2055 (2003).
3. Gordon, L. B. et al. Impact of farnesylation inhibitors on survival in Hutchinson–Gilford progeria syndrome. *Circulation* **130**, 27–34 (2014).
4. Gordon, L. B., Brown, W. T. & Collins, F. S. *Hutchinson–Gilford Progeria Syndrome* (GeneReviews, 2019).
5. Gaudelli, N. M. et al. Programmable base editing of A•T to G•C in genomic DNA without DNA cleavage. *Nature* **551**, 464–471 (2017).
6. Anzalone, A. V., Koblan, L. W. & Liu, D. R. Genome editing with CRISPR–Cas nucleases, base editors, transposases and prime editors. *Nat. Biotechnol.* **38**, 824–844 (2020).
7. Olive, M. et al. Cardiovascular pathology in Hutchinson–Gilford progeria: correlation with the vascular pathology of aging. *Arterioscler. Thromb. Vasc. Biol.* **30**, 2301–2309 (2010).
8. Gerhard-Herman, M. et al. Mechanisms of premature vascular aging in children with Hutchinson–Gilford progeria syndrome. *Hypertension* **59**, 92–97 (2012).
9. Rivera-Torres, J. et al. Cardiac electrical defects in progeroid mice and Hutchinson–Gilford progeria syndrome patients with nuclear lamina alterations. *Proc. Natl Acad. Sci. USA* **113**, E7250–E7259 (2016).
10. Prakash, A. et al. Cardiac abnormalities in patients with Hutchinson–Gilford progeria syndrome. *JAMA Cardiol.* **3**, 326–334 (2018).
11. Stehbens, W. E., Wakefield, S. J., Gilbert-Barness, E., Olson, R. E. & Ackerman, J. Histological and ultrastructural features of atherosclerosis in progeria. *Cardiovasc. Pathol.* **8**, 29–39 (1999).
12. Gordon, L. B. et al. Clinical trial of a farnesyltransferase inhibitor in children with Hutchinson–Gilford progeria syndrome. *Proc. Natl Acad. Sci. USA* **109**, 16666–16671 (2012).
13. Capell, B. C. & Collins, F. S. Human laminopathies: nuclei gone genetically awry. *Nat. Rev. Genet.* **7**, 940–952 (2006).
14. Lai, W.-F. & Wong, W.-T. Progress and trends in the development of therapies for Hutchinson–Gilford progeria syndrome. *Aging Cell* **19**, e13175 (2020).
15. Beyret, E. et al. Single-dose CRISPR–Cas9 therapy extends lifespan of mice with Hutchinson–Gilford progeria syndrome. *Nat. Med.* **25**, 419–422 (2019).
16. Santiago-Fernández, O. et al. Development of a CRISPR/Cas9-based therapy for Hutchinson–Gilford progeria syndrome. *Nat. Med.* **25**, 423–426 (2019).
17. Suzuki, K. et al. Precise in vivo genome editing via single homology arm donor mediated intron-targeting gene integration for genetic disease correction. *Cell Res.* **29**, 804–819 (2019).
18. Scaffidi, P. & Misteli, T. Reversal of the cellular phenotype in the premature aging disease Hutchinson–Gilford progeria syndrome. *Nat. Med.* **11**, 440–445 (2005).
19. Jiang, F. & Doudna, J. A. CRISPR–Cas9 structures and mechanisms. *Annu. Rev. Biophys.* **46**, 505–529 (2017).
20. Pattanayak, V. et al. High-throughput profiling of off-target DNA cleavage reveals RNA-programmed Cas9 nuclease specificity. *Nat. Biotechnol.* **31**, 839–843 (2013).
21. Komor, A. C., Kim, Y. B., Packer, M. S., Zuris, J. A. & Liu, D. R. Programmable editing of a target base in genomic DNA without double-stranded DNA cleavage. *Nature* **533**, 420–424 (2016).
22. Varga, R. et al. Progressive vascular smooth muscle cell defects in a mouse model of Hutchinson–Gilford progeria syndrome. *Proc. Natl Acad. Sci. USA* **103**, 3250–3255 (2006).
23. Huang, T. P. et al. Circularly permuted and PAM-modified Cas9 variants broaden the targeting scope of base editors. *Nat. Biotechnol.* **37**, 626–631 (2019).
24. Koblan, L. W. et al. Improving cytidine and adenine base editors by expression optimization and ancestral reconstruction. *Nat. Biotechnol.* **36**, 843–846 (2018).
25. Kleinstiver, B. P. et al. High-fidelity CRISPR–Cas9 nucleases with no detectable genome-wide off-target effects. *Nature* **529**, 490–495 (2016).
26. Tsai, S. Q. et al. CIRCLE-seq: a highly sensitive in vitro screen for genome-wide CRISPR–Cas9 nuclease off-targets. *Nat. Methods* **14**, 607–614 (2017).
27. Eisenberg, E. & Levanon, E. Y. A-to-I RNA editing—immune protector and transcriptome diversifier. *Nat. Rev. Genet.* **19**, 473–490 (2018).
28. Levy, J. M. et al. Cytosine and adenine base editing of the brain, liver, retina, heart and skeletal muscle of mice via adeno-associated viruses. *Nat. Biomed. Eng.* **4**, 97–110 (2020).
29. Villiger, L. et al. Treatment of a metabolic liver disease by in vivo genome base editing in adult mice. *Nat. Med.* **24**, 1519–1525 (2018).
30. Zincarelli, C., Soltys, S., Rengo, G. & Rabinowitz, J. E. Analysis of AAV serotypes 1-9 mediated gene expression and tropism in mice after systemic injection. *Mol. Ther.* **16**, 1073–1080 (2008).
31. Inagaki, K. et al. Robust systemic transduction with AAV9 vectors in mice: efficient global cardiac gene transfer superior to that of AAV8. *Mol. Ther.* **14**, 45–53 (2006).
32. Bostick, B., Ghosh, A., Yue, Y., Long, C. & Duan, D. Systemic AAV-9 transduction in mice is influenced by animal age but not by the route of administration. *Gene Ther.* **14**, 1605–1609 (2007).
33. Wang, L., Wang, H., Bell, P., McMenamin, D. & Wilson, J. M. Hepatic gene transfer in neonatal mice by adeno-associated virus serotype 8 vector. *Hum. Gene Ther.* **23**, 533–539 (2012).
34. Kessler, P. D. et al. Gene delivery to skeletal muscle results in sustained expression and systemic delivery of a therapeutic protein. *Proc. Natl Acad. Sci. USA* **93**, 14082–14087 (1996).
35. Nathwani, A. C. et al. Long-term safety and efficacy of factor IX gene therapy in hemophilia B. *N. Engl. J. Med.* **371**, 1994–2004 (2014).
36. Hagan, C. When are mice considered old? *The Jackson Laboratory* https://www.jax.org/news-and-insights/jax-blog/2017/november/when-are-mice-considered-old (2017).
37. Chandler, R. J., Sands, M. S. & Venditti, C. P. Recombinant adeno-associated viral integration and genotoxicity: insights from animal models. *Hum. Gene Ther.* **28**, 314–322 (2017).
38. Nault, J.-C. et al. Wild-type AAV insertions in hepatocellular carcinoma do not inform debate over genotoxicity risk of vectorized AAV. *Mol. Ther.* **24**, 660–661 (2016).
39. Geng, D., Zhao, W., Feng, Y. & Liu, J. Overexpression of Rab25 promotes hepatocellular carcinoma cell proliferation and invasion. *Tumour Biol.* **37**, 7713–7718 (2016).
40. Donsante, A. et al. Observed incidence of tumorigenesis in long-term rodent studies of rAAV vectors. *Gene Ther.* **8**, 1343–1346 (2001).
41. Donsante, A. et al. AAV vector integration sites in mouse hepatocellular carcinoma. *Science* **317**, 477 (2007).
42. Embury, J. E., Charron, C. C., Poirier, A. E. & Zori, A. Long term portal vein administration of AAV-WPRE vector results in increased incidence of neoplastic disease and hepatic pathology. *Mol. Ther.* **13**, S83 (2006).
43. Sands, M. S. AAV-mediated liver-directed gene therapy. *Methods Mol. Biol.* **807**, 141–157 (2011).
44. Richter, M. F. et al. Phage-assisted evolution of an adenine base editor with enhanced Cas domain compatibility and activity. *Nat. Biotechnol.* **38**, 883–891 (2020).
45. Gaudelli, N. M. et al. Directed evolution of adenine base editors with increased activity and therapeutic application. *Nat. Biotechnol.* **38**, 892–900 (2020).
46. Osorio, F. G. et al. Splicing-directed therapy in a new mouse model of human accelerated aging. *Sci. Transl. Med.* **3**, 106ra107 (2011).
47. Mateos, J. et al. Next-generation sequencing and quantitative proteomics of Hutchinson–Gilford progeria syndrome-derived cells point to a role of nucleotide metabolism in premature aging. *PloS One* **13**, e0205878 (2018).

Methods

Data reporting

Sample sizes were determined on the basis of literature precedence for genome editing experiments, and were justified by power calculation estimating 90% power to detect differential ages in longevity studies. The experiments were not randomized and the investigators were not blinded to allocation during experiments and outcome assessment.

Cell culture

HGADFN167 and HGADFN188 cells (Progeria Research Foundation) were maintained in antibiotic-free DMEM (Thermo Fisher Scientific10569044) supplemented with 20% (v/v) fetal bovine serum (Thermo Fisher), at 37 °C with 5% CO_2. HEK239T/17 (ATCC CRL-11268) cells were maintained in antibiotic-free DMEM (Thermo Fisher Scientific 10569044) supplemented with 10% (v/v) fetal bovine serum (Thermo Fisher Scientific), at 37 °C with 5% CO_2.

Lentiviral vector cloning

The ABEmax-VRQR gene was inserted into the lentiCRISPRv2 backbone (Addgene 52961) via restriction cloning. Backbone plasmid was digested using AgeI and BamHI according to the manufacturer's protocol. ABEmax-VRQR was amplified from (Addgene 119811) using the primers LWK901 and LWK902. Gibson assembly was performed using a 3:1 molar ratio of insert to vector backbone according to the manufacturer's protocol. The *LMNA* c.1824 C>T targeted sgRNA was installed by digesting the cloned backbone with BsmBI and gel-extracting the resulting cleaved backbone. DNA oligonucleotides encoding the sgRNA were ordered to match the corresponding overhangs generated by BsmBI digestion (5′-CACCGGTCCACCCACCTGGGCTCC-3′ and 5′-AAACGGAGCCCAGGTGGGTGGACC-3′). Oligonucleotides were annealed and phosphorylated using T4-PNK according to the manufacturer's instructions and ligated into the digested backbone as previously described[24]. LWK901: 5′-TTTGCCGCCAG AACACAGGACCGGT GCCACCATGAAACGGACAGCCGACG-3′; LWK902: 5′-GGGAAAAGTT GGTGGCCCCGGATCCGACTTTCCTCTT CTTCTTGGGCTCG-3′.

AAV vector cloning

N-terminal virus was as previously reported[28]. C-terminal virus required the installation of the VRQR mutations (D1135V, G1218R, R1335Q, T1337R) as well as the sgRNA sequence targeting *LMNA* c.1824 C>T. The VRQR mutations were installed by Gibson assembly and ligation of the ABEmax-VRQR C terminus. The sgRNA targeting *LMNA* c.1824 C>T was installed by BsmBI digestion of the backbone as described for the lentiviral backbone and ligation of the same top and bottom oligonucleotides into the cut vector.

To generate the C-terminal AAV genome encoding Npu-ABEmax (VRQR) and the sgRNA targeting *LMNA* G608G, we first subcloned Npu-ABEmax(VRQR) in a mammalian (CMV) expression plasmid by deleting the UGI domains from an Npu-BE4max(VRQR) intermediate. We then amplified by PCR the Npu-ABEmax(VRQR) gene using primers 877(fwd)/670(rev) and cloned by Gibson assembly into AgeI/BglII-cut AAV plasmid. In a subsequent cloning step, annealed oligonucleotides encoding the sgRNA targeting *LMNA* G608G were ligated into BsmBI-cut plasmid. 877(fwd): 5′-TCACTTTTTTTCAGGTTGGACCGGT GCCACCATGAAACGGACAGCCGACGG-3′; 670(rev): 5′-AATCCAGAGGTT GATTATCAGATCTTAGACTTTCCTCTTCTTCTTGGGCTCG AATTCGC-3′.

Lentiviral production

HEK239T/17 (ATCC CRL-11268) cells were maintained in antibiotic-free DMEM (Thermo Fisher Scientific 10569044) supplemented with 10% (v/v) fetal bovine serum (Thermo Fisher Scientific), at 37 °C with 5% CO_2. Cells were verified to be free of mycoplasma by ATCC upon purchase. On day 1, cells were split 1:3 from rapidly dividing HEK293T/17 flasks that had been split 1:10 three days prior. The following day, the medium was changed on cells and cells were transfected using FuGENE HD according to the manufacturer's protocol. Transfection mix included 9 µg of transfer vector (the packaging genome of interest), 9 µg of psPAX2 (encoding the viral packaging proteins) and 6 µg of pVSV-G (encoding the VSV-G envelope protein). Transfection mix was then supplemented with 70 µl of room temperature equilibrated FuGENE and brought to a final volume of 1,500 µl per flask with Opti-MEM. Two days after transfection, medium was collected and spun at 3,000*g* for 15 min to remove remaining cells. Centrifuged supernatant was passed through a 0.45-µm PVDF filter to eliminate all non-viral debris. Supernatant was transferred directly to target cells.

The human non-targeting control sgRNA sequence was used from a previous study[48]. Oligos containing these non-targeting sgRNAs with 5′ overhang BsmBI digestion sites were synthesized by Integrated DNA Technologies. The oligos were first annealed and inserted into the lentiCRISPR v2 plasmids (a gift from F. Zhang, Addgene plasmid 52961) as previously described[49]. The fragments containing these non-targeting sgRNAs were digested from the recombinant lentiCRISPR v2 plasmids by restriction enzymes KpnI and NheI. These fragments were then ligated into the ABEmax7.10 backbone, which was extracted from the digests of KpnI and NheI. The sequences of the recombinant plasmids were confirmed by Sanger sequencing. Control sgRNA oligonucleotide sequences: ctrl sgRNA F 5′-CACCGGCCTGCCCTAAACCCCGGAA-3′; ctrl sgRNA R 5′-AACTTCCGGGGTTTAGGGCAGGCC-3′.

HGADFN167 and HGADFN188 lentiviral transduction

Lentivirus was generated as described above. HGADFN167 and HGADFN188 cells were cultured in 75-cm flasks in antibiotic-free DMEM supplemented with 20% FBS. Supernatant was removed from cells and medium was replaced with 15 ml filtered lentiviral medium per plate, supplemented with 5 ml of regular DMEM. Cells were grown for 3 days before medium change with DMEM + 20% FBS including 2 µg/ml puromycin to select for cells expressing full-length editor. Cells were maintained in selective medium for 10 and 20 days post-infection before collecting genomic DNA, RNA and protein while also isolating cells at 20 days of age for histological analysis.

HGADFN167 and HGADFN188 genomic DNA isolation

Genomic DNA for DNA sequencing analysis was isolated first by trypsinizing cells and centrifugation of one 15-cm dish per cell line per time point. Trypsinized cells were resuspended in medium and spun gently at 100*g* for 10 min. Cell pellets were resuspended in 200 µl of lysis buffer (10 mM Tris-HCl, pH 7.5, 0.05% SDS, 25 µg/ml proteinase K (NEB)). Lysing cells were incubated at 37 °C for 1 h. Proteinase K was inactivated by 30-min incubation at 80 °C.

HGADFN167 and HGADFN188 RNA extraction and ddPCR

Total RNA from the cell lines was extracted with Trizol (Life Technologies) and purified using the RNeasy mini kit (Qiagen) per the manufacturer's instructions. The total RNA yield was determined using the NanoDrop 2000 spectrophotometer. One microgram of total RNA per condition was converted to cDNA using the iScript Select cDNA Synthesis Kit (Bio-Rad). PCR cycling conditions consisted of an initial enzyme activation step for 10 min at 95 °C, followed by 40 cycles of 94 °C for 30 s and 59 °C for 30 s with a 2 °C/second ramp rate, and a 10-min enzyme deactivation step at 98 °C for 10 min. Each reaction was duplexed with the Human TFRC PrimePCR Probe Assay (assayID qHsaCIP0033292, HEX) and performed in triplicate. After completion of reactions, samples were analysed on a QX200 droplet reader (BioRad) to obtain expression levels relative to mouse *Hprt* and transcript-specific copy number, then further analysed using Excel software.

Cell line qPCR analysis

RT–qPCR was performed in triplicate using SYBR Green Supermix (Bio-Rad) on CFX96 real-time system (C1000 Thermal Cycler; Bio-Rad).

The relative mRNA level of *LMNA* and progerin is normalized to *GAPDH*, a housekeeping gene used as an internal control. Primers for *GAPDH* were obtained from OriGENE Technologies. For amplifying *LMNA* transcript, the forward PCR primer was 5′-GCAACAAGTCCAATGAGGACCA-3′ and the reverse primer was 5′-CATGATGCTGCAGTTCTGGGGGCTCTGGAT-3′; for progerin mRNA amplification, the sequence of the forward PCR primer was 5′-GCAACAAG TCCAATGAGGACCA-3′ and the reverse primer was 5′-CATGATGCTGCAGTTCTGGGGGCTCTGGAC-3′.

HGADFN167 and HGADFN188 RNA-seq analysis

Total RNA was applied to Oligo-dT(25) Dynabeads (Thermo Fisher Scientific) to enrich for polyadenylated transcripts. Stranded RNA-seq libraries were generated using the PrepX mRNA 48 kit (Takara) on the Apollo 324 automated liquid handling system (Wafergen) followed by barcoding and amplification (12 cycles). Following PCR and bead clean-up with AmpureXP beads (Beckman Coulter), libraries were visualized on a 4200 TapeStation system (Agilent) and quantified using a Library Quantification Kit (KAPA Biosystems). Libraries were sequenced on a NextSeq high-throughput flow cell (Illumina) as 75-bp paired-end reads. All raw fastq files generated are available from the NCBI Sequence Read Archive (SRA) under BioProject PRJNA627465.

Fastq files were generated with bcl2fastq2 v.2.20 and trimmed using TrimGalore v.0.6.2 to remove low-quality bases, unpaired sequences and adaptor sequences. Trimmed reads were aligned to *Homo sapiens* genome assembly GRCh38 with a custom Cas9-ABEmax gene entry by initially aligning with STAR (v.2.7.3a) to identify splice junctions followed by an additional STAR alignment including the splice junctions identified in the first STAR alignment (2-STAR pass).

To calculate the average percentage of A-to-I editing amongst adenosines sequenced in transcriptome-wide sequencing analysis, we used REDItools v.1.3 to quantify the percentage editing in each sample. We removed all nucleotides except adenosines from our analysis and then removed all adenosines with a read coverage less than 10 to avoid errors due to low sampling; in addition, we removed positions with a mapping or read quality score below 25. Next, we calculated the number of adenosines converted to inosine in each sample and divided this by the total number of adenosines in our dataset after filtering to obtain a percentage of adenosines edited to inosine in the transcriptome. The standard error of the mean (s.e.m.) was calculated by comparison of three biological replicates. Significance was calculated using the student's unpaired *t*-test.

Transcriptome correction analysis in progeria cell lines

Treated HGADFN167 and HGADFN188 cells at 10-day and 20-day time points were used for analysis. Untreated HGADFN167 and HGADFN188 cells were also used. Untreated unaffected donor cells (AG03257) were obtained from Coriell Cell Bank and were also used for analysis. Additional unaffected cells were also pulled from a previous study and used for analysis[47].

Sorted bam files generated in the 2-STAR pass alignment described above were supplied to RSEM version 1.3.1 to count transcripts. The limma-voom R package was used to normalize gene expression levels and perform differential expression analysis. Gene ontology molecular function analysis of differentially expressed genes was performed as previously described[50].

HGADFN167 and HGADFN188 protein isolation and western blot analysis

HGPS fibroblasts were prepared by collecting cells with trypsin, washing briefly in cold PBS and then lysing in RIPA lysis buffer (150 mM NaCl, 50 mM Tris-HCL pH8, SDS 1%, sodium deoxycholic acid 0.5%, NP-40 1%) for 30 min. After high-speed centrifugation at 4 °C for 15 min, protein was quantified using standard BCA. Lysates were diluted in LDS sample buffer and heated at 70 °C for 10 min and separated by SDS–PAGE on 4–12% Bis-Tris gels (Nupage, Invitrogen). Protein was transferred to a nitrocellulose membrane using a Mini Gel Tank for 90 min at 30 V. Membranes were blocked with Intercept TBS Blocking Buffer (LI-COR) and primary antibodies were incubated overnight in Intercept buffer. Membranes were then washed 3 times for 10 min in TBS-T (0.1% Tween) and incubated with IRDye conjugated secondary antibodies at 1:10,000 dilution (LI-COR). The following antibodies were used for cell and tissue blotting: anti-lamin A/C, which recognizes human lamin A/C and progerin (Abcam 40567, Jol2 Clone, 1:200); anti-β-actin (Abcam 8227, 1:1,000); anti-histone 3 (Cell Signaling Technology 4499, 1:2,000). Goat anti-rabbit secondary (IRDye 680LT) or goat anti-mouse secondary (IRDye 800cw) were used at 1:10,000 dilution.

Western blot densitometry was performed to quantify relative protein abundance for in vivo samples. The relative abundance of lamin A or progerin protein in saline- or ABE-treated samples was quantified by normalizing densitometry values for each band to its corresponding β-actin band.

For Extended Data Fig. 1e, g, whole-cell lysates were prepared by dissolving cell pellets in Laemmli Sample Buffer containing 5% 2-mercaptoethanol (Bio-Rad). Subsequently, protein samples were resolved on 10% SDS–PAGE gels and transferred onto nitrocellulose membranes (Bio-Rad). Antibodies used in this study were lamin A/C (MAB3211; Millipore; 1:500 dilution), progerin (Collins, custom; 1:500 dilution) and GAPDH (SC-47724, Santa Cruz; 1:5,000 dilution). Secondary antibodies used for these blots were anti-mouse (SC-516102, Santa Cruz) and anti-rabbit (211-035-109, Jackson ImmunoResearch), both at 1:5,000 dilutions.

HGADFN167 and HGADFN188 immunocytochemistry

For immunocytochemistry, cells were fixed in 4% paraformaldehyde (PFA) for 15 min. The cells were then blocked with 4% BSA serum in tris-buffered saline (TBS) for 1 h. Subsequently, the cells were incubated with the primary antibodies lamin A/C (MAB3211; Millipore; 1:250 dilution) and progerin[51] (Collins, custom; 1:250 dilution) in 4% BSA in TBS (0.3% Triton-X) overnight at 4 °C. After three washes with TBS, cells were incubated in 1% BSA in TBS containing secondary antibodies and DAPI (Vector Laboratories). Secondary antibodies used were Alexa Fluor 594 donkey anti-rabbit IgG (Invitrogen) and Alexa Fluor 488 donkey anti-mouse IgG (Invitrogen) (both at 1:1,000 dilution). Images were acquired with Zeiss AX10 microscope equipped with a SPOT Pursuit camera. More than 150 nuclei were analysed per condition, whereby nuclei were assigned by visual inspection into abnormal or normal bins on the basis of nuclear blebbing phenotype.

Cell line high-throughput sequencing and data analysis

Genomic DNA was amplified by qPCR using Phusion Hot Start II DNA polymerase with use of SYBR gold for quantification. DMSO (3%) was added to all gDNA PCR reactions. To minimize PCR bias, reactions were stopped during the exponential amplification phase. One microlitre of the unpurified gDNA PCR was used as a template for subsequent barcoding PCR (10 cycles, annealing temperature 61 °C). Pooled barcoding PCR products were gel-extracted (Min-elute columns, Qiagen) and quantified by qPCR (KAPA KK4824) or Qubit dsDNA HS assay kit (Thermo Fisher Scientific). Sequencing of pooled amplicons was performed using an Illumina MiSeq according to the manufacturer's instructions. Oligonucleotide sequences for the primers used are provided below.

Initial de-multiplexing and fastq generation were performed by bcl2fastq2 running on BaseSpace (Illumina) with the following flags: –ignore-missing-bcls –ignore-missing-filter –ignore-missing-positions –ignore-missing-controls –auto-set-to-zero-barcode-mismatches –find-adapters-with-sliding-window –adaptor-stringency 0.9 –mask-short-adaptor-reads 35 –minimum-trimmed-read-length 35. Alignment of fastq files and quantification of editing frequency was performed by CRISPResso2 in batch mode with a window width of 10 nucleotides. Human *LMNA*-specific primers are as follows (Illumina MiSeq adaptor sequences in bold): forward: 5′-**ACACTCTTTCCCTACACGACGCT**

CTTCCGATCTNNNNACCCCGCTGAGTACAACC-3′; reverse: 5′-**TGGAGTTCAGACGTGTGCTCTTCCGATCTNNNN**GCAGAAGAGCCAGAGGAGAT-3′.

Cas9-VRQR nuclease purification

Cas9-VRQR nuclease was cloned into a pET42b plasmid with a 6×His tag, eliminating the normal glutathione-*S*-transferase fusion. BL21 Star DE3 chemically competent *Escherichia coli* cells (Invitrogen) were transformed with the plasmid and picked into 2×YT+25 μg/ml kanamycin for overnight growth at 37 °C. The next day, 1 l of pre-warmed 2×YT+25 μg/ml kanamycin was inoculated at an optical density at 600 nm (OD_{600}) = 0.03 and shaken at 37 °C for about 3 h until OD_{600} reached 0.8. Culture was cold-shocked in an ice-water slurry for one hour, after which protein expression was induced by the addition of 1 mM IPTG. Culture was shaken at 16 °C for 16 h to express protein. Cells were pelleted at 6,000*g* for 20 min and stored at −80 °C. The next day, cells were resuspended in 30 ml cold lysis buffer (1 M NaCl, 100 mM Tris-HCl pH 7.0, 5 mM TCEP, 20% glycerol, with 3 tablets of cOmplete, EDTA-free protease inhibitor cocktail (Millipore Sigma, 4693132001). Cells were lysed by sonification at 4 °C for a total treatment of 7.5 min, providing time to cool after every 3 s of treatment. Cell lysate was clarified for 20 min using a 20,000*g* centrifugation at 4 °C. Supernatant was collected and added to 1.5 ml of Ni-NTA resin slurry (G Bioscience, 786-940, prewashed once with lysis buffer). Protein-bound resin was washed twice with 12 ml of lysis buffer in a gravity column. Protein was eluted in 3 ml of elution buffer (200 mM imidazole, 500 mM NaCl, 100 mM Tris-HCl pH 7.0, 5 mM TCEP, 20% glycerol). Eluted protein was diluted in 40 ml of low-salt buffer (100 mM Tris-HCl, pH 7.0, 5 mM TCEP, 20% glycerol) just before loading into a 50-ml Akta Superloop for ion-exchange purification on the Akta Pure25 FPLC. Ion-exchange chromatography was conducted on a 5-ml GE Healthcare HiTrap SP HP pre-packed column. After washing the column with 15 ml low salt buffer, the diluted protein was flowed through the column to bind. The column was washed in 15 ml of low-salt buffer before being subjected to an increasing gradient to a maximum of 80% high-salt buffer (1 M NaCl, 100 mM Tris-HCl, pH 7.0, 5 mM TCEP, 20% glycerol) over the course of 50 ml, at a flow rate of 5 ml per minute. One-millilitre fractions were collected during this ramp to high-salt buffer. Peaks were assessed by SDS–PAGE to identify fractions containing the desired protein, which were pooled and concentrated using an Amicon Ultra 15-ml centrifugal filter (100 kDa cut-off). SDS–PAGE stained with InstantBlue (Expedion, SKU ISB1L) was used to visualize the purity after each step (Extended Data Fig. 2c). Concentrated protein was quantified using a BCA assay (Thermo Fisher Scientific, 23227); the final concentration was 68.6 μM.

CIRCLE-seq sample preparation and off-target analysis

Genomic DNA was isolated from both HGADFN167 and HGADFN188 cell lines using a Gentra Puregene Tissue Kit (Qiagen). CIRCLE-seq was performed as previously described[26]. Cas9-VRQR was complexed with a synthetic sgRNA (Synthego) containing phosphorothioate linkage and 2′MeO modification at the first and last three nucleotides, and this complex was used to treat circularized DNA. PCR amplification before sequencing was conducted using PhusionU polymerase. PCR product was gel-purified and quantified by QuBit dsDNA high-sensitivity assay (Invitrogen) before loading onto an Illumina MiSeq. Data were processed using the CIRCLE-Seq analysis pipeline (https://github.com/tsailabSJ/circleseq) with parameters: 'read_threshold: 4; window_size: 3; mapq_threshold: 50; start_threshold: 1; gap_threshold: 3; mismatch_threshold: 6; merged_analysis: True'. The human reference genome GRCh37 was used for alignment. The 20 off-target genomic loci that yielded the greatest read counts for each sample were chosen for more detailed analysis. Loci tied for the highest read counts were included, and 7 loci were shared in the top 20 list from each cell line, thus primers were designed to amplify 35 sites in total. Of these, PCR product was successfully obtained for 32 sites. These PCR products of edited and unedited cells were sequencing using an Illumina MiSeq. For successfully amplified loci, amplicons were aligned using CRISPResso2 as with other amplicon sequencing performed in this manuscript; however, these samples were stringently quality filtered with a flag for $q = 30$ to ensure single-nucleotide polymorphism (SNP) calling was only performed on high-quality reads. The resulting data are in Supplementary Data 4.

AAV production

AAV production was performed as previously described[28]. In brief, HEK293T/17 cells were maintained in DMEM/10% FBS without antibiotic in 150-mm dishes (Thermo Fisher Scientific 157150) and passaged every 2–3 days. Cells for production were split 1:3 and allowed to grow near 100% confluent before PEI transfection the following day. Per plate, 5.7 μg AAV genome, 11.4 μg pHelper (Clontech) and 22.8 μg rep-cap plasmid were transfected. One day after transfection, medium was exchanged for DMEM/5% FBS. Three days after transfection, cells were scraped with a rubber cell scraper (Corning), pelleted by centrifugation for 10 min at 2,000*g*, resuspended in 500 μl hypertonic lysis buffer per plate (40 mM Tris base, 500 mM NaCl, 2 mM $MgCl_2$ with 100 U/ml salt active nuclease (Arcticzymes 70910-202)), and incubated at 37 °C for 1 h to lyse cells. Medium was decanted, combined with a 5× solution of 40% PEG/2.5 M NaCl (final concentration 8% PEG/500 mM NaCl), incubated on ice for 2 h to facilitate PEG precipitation, and centrifuged at >3,000*g* for 40 min. The supernatant was discarded and the pellet resuspended in 500 μl lysis buffer per plate and added to the cell lysate. Incubation at 37 °C was continued for 30 min. Crude lysates were either incubated at 4 °C overnight or directly used for ultracentrifugation.

Cell lysates were gently clarified by centrifugation at 2,000*g* for 10 min and added to Beckman Quick-seal tubes via 16-gauge disposable needles (Air-Tite N165). A discontinuous iodixanol gradient was formed by sequentially floating layers: 9 ml 15% iodixanol in 500 mM NaCl and 1× PBS-MK (1× PBS plus 1 mM $MgCl_2$ and 2.5 mM KCl), 6 ml 25% iodixanol in 1× PBS-MK, and 5 ml each of 40% and 60% iodixanol in 1× PBS-MK. Phenol red (1 μg/ml final) was added to the 15, 25 and 60% layers to facilitate identification. Ultracentrifugation was performed using a Ti 70 rotor at 58,600 rpm for 2 h 15 min at 18 °C. After ultracentrifugation, roughly 4 ml of solution was withdrawn from the 40–60% iodixanol interface via an 18-gauge needle, dialysed with PBS containing 0.001% F-68 and ultrafiltered via 100-kDa MWCO columns. The concentrated viral solution was sterile-filtered using a 0.22-μm filter, quantified via qPCR (Clontech AAVpro Titration Kit v.2) and stored at 4 °C until use.

Timing of 6-month tissue and longevity analysis

The 6-month time point was chosen as a time when untreated homozygous *LMNA* c.1824 C>T mice typically show phenotypic decline but are not yet at the end of their median lifespan (7.0 months, females; 7.3 months, males).

High-throughput sequencing of in vivo samples

Genomic DNA was isolated by standard protocol using extraction, tissue preparation, and neutralization solution (Sigma-Aldrich) from 5- to 10-mg tissue samples. Isolated DNA was amplified as described for the genomic DNA samples using the same PCR1 and PCR2 primers. Libraries were prepared, diluted and sequenced on an Illumina MiSeq as previously described[28].

To guarantee that only reads belonging to the human *LMNA* gene were included for downstream analysis first, UCHIME v.4.2 was used to remove PCR-generated chimaeras. Sequences were further filtered by removing reads containing at least two sequence motifs unique to mouse LMNA. Code is available at the link in Supplementary Note 3. Resulting reads were aligned and the editing frequency quantified by CRISPResso2 in batch mode with a window width of 10 nucleotides.

RNA isolation and ddPCR from mouse tissues

Mouse tissues were collected into Trizol reagent (Thermo Fisher Scientific), homogenized and immediately flash-frozen until ready for total RNA isolation. RNA was subsequently digested for 20 min at 37 °C with recombinant DNase I (Thermo Fisher Scientific), then analysed for integrity and concentration on an Agilent nucleic acid bioanalyzer (Agilent Technologies). Synthesis of cDNA used 1 µg of RNA, which was reverse-transcribed using the iScript cDNA Synthesis kit (BioRad) according to the manufacturer's protocol. For each transcript assay, droplets were generated using 50 ng of cDNA, 900 nM primers, 250 nM probes in 1× ddPCR Supermix for Probes (BioRad) on a QX200 Droplet Generator, followed by PCR amplification. The sequence of primers and probes used are listed in the appended table. PCR cycling conditions consisted of an initial enzyme activation step for 10 min at 95 °C, followed by 40 cycles of 94 °C for 30 s and 59 °C for 30 s with a 2 °C/second ramp rate, and a 10 min enzyme deactivation step at 98 °C for 10 min. Each reaction was duplexed with the Mouse Hprt PrimePCR Probe Assay (assay ID qMmuCEP0054164, HEX, BioRad) and performed in triplicate. After completion of reactions, samples were read on a QX200 droplet reader (BioRad) to obtain expression levels relative to mouse *Hprt* and transcript-specific copy number, then further analysed using Excel software.

The following primers were used to probe human *LMNA*: hLMNA-F: 5′-CCCAGGTGG GCGGAC-3′; hLMNA-R: 5′-AGGAGCGGG TGACCAGATT-3′; and hLMNA-FAM: 5′-56-FAM-CAGCTACCGC AGTGTGGGGG-IABkFQ-3′. The following primers were used to probe human progerin: hPROG-F: 5′-CTGTGCGG GACCTGCG-3′; hPROG-R: 5′-AAGCCTCCAC CCCCACC-3′; and hPROG-FAM: 5′-56-FAM-AGGAGCCCAA GCCCCCAGAACT-IABkFQ-3′. The following primers were used to probe human *LMNC*: hLMNC-F: 5′GTGGAAGGCA CAGAACACCT-3′; hLMNC-R: 5′CATTCTTTAAT GAAAAGATTTTTGG-3′; and hLMNC-FAM: 5′-56-FAM-CAGTGACTGTGGT TGAGGACGACG-IABkFQ-3′.

Protein isolation and western blotting from mouse tissues

After euthanasia, tissues from control or ABE-treated mice were flash-frozen and stored in liquid nitrogen until the time of protein extraction. To extract proteins, 10–30 mg of frozen tissue was first pulverized in temperature-resistant tubes (Covaris, tissueTUBE 520001) on a liquid nitrogen bath. This frozen tissue powder was resuspended in RIPA lysis buffer (see above), moved to a 2-ml collection tube and homogenized for 30 s at 25 Hz with a 5-mm stainless steel bead in a TissueLyser II (Qiagen). Samples were then centrifuged for 5 s on table-top microcentrifuge and incubated on ice for 45 min while rocking. After incubation, lysates were clarified by centrifugation at 21,000*g* for 15 min at 4 °C. The supernatant was transferred to a fresh tube and protein quantified using a standard BCA assay. Tissue lysates were prepared identically to the cell line isolated samples and separated by SDS–PAGE (25 µg protein loaded for heart and liver; 10 µg for skeletal muscle; 7.5 µg for aorta, 7.5 µg for cells) on 4–12% Bis-Tris gels (Nupage, Invitrogen). Tissue western blots were performed using the same method as cell line western blots.

Tissue histology

Tissues were fixed in 2% PFA for 24 h before dehydration with graded alcohols and embedding in paraffin. Cross-sections (4-µm thick) were cut and mounted on charged slides and visualized by H&E staining. For aorta and skin sections, additional staining was performed with Movat's pentachrome (CVPath) or Masson's trichrome (Histoserv), respectively. Images were captured on an Axioscan imaging system (Zeiss) at 20× magnification and processed using ZenBlue 2.0 software. Images were further processed for VSMC counts and adventitial area assessment using Photoshop CC software (v.21.2.3).

Immunofluorescence histochemistry

Immunohistostaining was performed following the protocol previously described[7] with modifications, and by using mouse monoclonal anti-lamin A/C (MABT538, clone 2E8.2, Millipore Sigma; 1:75 dilution) antibody or rabbit polyclonal anti-progerin antibody (Collins, custom; 1:75 dilution). In brief, ascending aorta sections were dewaxed and rehydrated, and the antigens were retrieved by heating in EDTA buffer (1 mM, pH 8.0) for 2 min in a pressure cooker. Tissue sections were blocked in TBS buffer containing 10% donkey serum and 1% BSA, and then incubated with a mouse-on-mouse blocking reagent (Vector Laboratories) to reduce endogenous mouse antibody binding. Slides were incubated with the above primary antibody overnight at 4 °C. After washing thoroughly in TBS, the sections were then incubated with donkey anti-mouse Alexa Fluor 594-conjugated or donkey anti-rabbit Alexa Fluor 488-conjugated secondary antibodies (Thermo Fisher Scientific; 1:3,000 dilutions). All tissue sections were mounted in DAPI-containing medium (Vector Laboratories). Fluorescence images were captured by a confocal microscope system (Zeiss LMS 880) with a 40× water lens.

Whole-genome sequencing of isolated tumour samples

Tumours were isolated from mouse livers following standard necropsy of deceased mice. After tissue isolation, genomic DNA was isolated using the QIAamp DNA Mini Kit (Qiagen) according to the manufacturer's recommendations. The resulting isolated genomic DNA was sheared to a mean size of 300 bp using a Covaris S220 sonicator (Covaris). An Illumina sequencing library was prepared from the sheared DNA using the Apollo 324 automated liquid handler (WaferGen) and the PrepX DNA library kit (Takara Bio). This step included DNA end repairing, A-tailing, adaptor ligation, barcoding and 5 cycles of PCR amplification. After examination on a TapeStation 4200 system (Agilent) with a high-sensitivity DNA 1000 ScreenTape (Agilent) for size distribution, and library concentration quantification by Qubit fluorometer (Invitrogen), the resulting libraries were pooled and sequenced on an Illumina Novaseq using an S4 flow cell as paired-end 150-bp reads, along with 6-bp index reads, following the manufacturer's protocol (Illumina).

Quality control of sequence reads

We assessed sequence quality of the paired-end reads with FastQC (v.0.10.0, http://www.bioinformatics.babraham.ac.uk/projects/fastqc/) for each of 16 whole-genome samples. Sequencing of a second tumour sample from mouse 9550 failed, and the sample was excluded from analysis. Singleton reads were not included in the FastQC analysis, and they were excluded from alignment (see below) and downstream variant calling. We used MultiQC[52] (v.1.8) to summarize the FastQC results. No outlier sample was detected in the evaluation of mean base quality and mapping quality across the samples.

Sequence alignment and variant calling

We assembled a comprehensive reference genome including the following components: (1) the mouse genome GRCm38; (2) AAV9 C-terminal contig; (3) AAV9 N-terminal contig; (4) cloning vector pBACe3.6 (GenBank U80929.2)[53]; and (5) RP11-702H12, a human *LMNA* BAC sequence present in the transgenic mouse model[54]. Each of the four non-mouse components was integrated in the reference genome as a separate contig. The alignment program 'bwa mem'[55] (v.0.7.17) was used to align the sequence reads to the combined reference genome with '-M' option, and the remaining parameters were set to default. On average, 1,542,162,680 sequence reads (≥548,801,830) per sample were generated, of which 99.58% mapped to the genome as primary alignments. For sequencing statistics, see the second tab of Supplementary Data 1.

Identification of AAV9 integration in mouse genomes

We implemented a two-step process to identify AAV9 integration sites in mice genomes. First, we used 'samtools view' (v.0.1.18)[56] to extract

any reads that map to AAV9 C- or N-terminal contigs. We excluded the following reads: (1) mapping quality score of less than 30; (2) failed Illumina platform/vendor quality check; and (3) duplicates. Next, we anchored the reads mapped to AAV9 contigs and searched the ones whose paired read mapped to the mouse genome. These read pairs represented sequencing fragments that cover potential integration sites of AAV9 contigs and mouse chromosomes.

We annotated the mouse genomic DNA reads identified around the integration sites with genes defined in GENCODE v.M24 (https://www.gencodegenes.org/pages/gencode.html) using 'bedtools intersect'[57]. To capture integration sites that were near, but not within, a gene body, we extended both ends of each mouse gene by 2 kb of flanking sequence for the purposes of this annotation. These steps resulted in a list of AAV9 contigs that are integrated into the mouse genome. The resulting data are in Supplementary Data 1.

Single-nucleotide variant calling from whole-genome sequencing data

Aligned reads were mapped to the reference genome as described above. Duplicates were removed using Sambamba[58] and the Genome Analysis Toolkit (GATK) was applied[59]. Base quality score recalibration, indel realignment, and SNP and indel discovery and genotyping of all 15 samples were performed simultaneously using standard hard-filtering parameters according to GATK best practices recommendations[60,61]. SNPs and indels were annotated using ANNOVAR[62]. To compare the fraction of all single-nucleotide variants (SNVs) that are A•T-to-G•C between different tissue samples, generalized linear models were fitted and FDR-adjusted *P* values were reported on three datasets: (1) three independent liver tumour samples and two independent saline-injected samples; (2) four independent normal liver samples and two saline-injected samples; and (3) seven liver tumour samples and six normal liver samples from four independent mice with mouse identity as a covariate. The resulting data are summarized in Supplementary Data 2, with the full dataset available in Supplementary Data 5.

Analysis of liver-cancer-associated genomic loci

Cancer-associated SNVs and indels were obtained from the COSMIC Cancer Mutation Census (https://cancer.sanger.ac.uk/cmc/home)[63]. This list was first filtered to identify recurrent or cancer associated mutations. These were defined by matching at least one of the following three criteria: (1) having greater than 1% prevalence in at least one tumour type as measured by whole-genome sequencing; (2) scoring as probably pathogenic or pathogenic on the basis of the ClinVar clinical significance criteria; and (3) having a dN/dS diseases score with a significant *q*-value (*q*-value < 0.05) in at least one tumour type as defined by COSMIC analysis of The Cancer Genome Atlas (TCGA) whole-exome data.

These criteria resulted in 19,986 high-confidence human cancer-associated mutations spanning 6,614 genes and 171 liver cancer-associated mutations spanning 84 genes. High-confidence human liver cancer-associated mutations included those affecting many well-known genes implicated in liver cancer such as *HNF1A*, *CTNNB1* (β-catenin) and *IL6ST* (interleukin 6 signal transducer). This analysis did not include copy number or structural variants.

Whole-genome sequencing GATK ANNOVAR analysis output from mouse liver and tumour samples (see above) was first filtered for variants not found in both saline-treated mouse livers, and then further filtered to only include indels and events associated with adenine base editing (A>G and *T*>C mutations).

These mutations were then classified based on the following: (1) mutations falling within the coding region or affecting the splicing of a gene with known high-confidence cancer-associated mutations (denoted as CODING); or (2) mutations not in the first category that reside in an active *cis*-regulatory region within 100 kb of a gene with known high-confidence cancer-associated mutations (denoted as REGULATORY). Active *cis*-regulatory regions were defined using ATAC-seq (a measure of open and active regulatory chromatin)[64] in postnatal mouse livers from a processed dataset generated by the mouse ENCODE project (https://www.encodeproject.org/files/ENCFF168WUC/). This definition resulted in 24,758 ATAC-seq-defined mouse liver *cis*-regulatory regions within 100 kb of high-confidence cancer-associated genes and 526 *cis*-regulatory regions associated with liver cancer-specific genes. The resulting data are in Supplementary Data 3.

RAB25 transcript detection

RNA was isolated from liver samples as described above and reverse-transcribed using the iScript cDNA Synthesis kit (BioRad) according to the manufacturer's protocol. PCR was performed using gene-specific primers for mouse *Gapdh* (Biorad; 10031231), mouse *Actb* (Biorad; 10031237) and human *RAB25* (Biorad; 10031234) with the iQ multiplex powermix (Biorad). PCR products were analysed by gel electrophoresis on a 2% agarose gel.

Mice

Mice were housed in barrier facilities with a 12-h light–dark cycle at the National Institutes of Health (NIH) and Vanderbilt University Medical Center (VUMC). Genotyping was performed using standard PCR methods with the following primers: 5′-TTGGACCAAACAAGTACATATCA-3′ (common forward); 5′-CCAATGATAGTGACAGGTATACGG-3′ (wild-type reverse); 5′-CTGACATTCTAGTGGAGGGAGA-3′ (mutant reverse). Body weights were measured and recorded during health observation twice per week. Mice were injected with split AAV constructs at P3 (retro-orbital, 10^{11} vg total in 10 µl total volume) or P14 (retro-orbital and intraperitoneal, 10^{12} vg total in 100 µl total volume). All retro-orbital injections were performed at NIH, and intraperitoneal injections were done at VUMC. Full pathological examination included the ascending aorta, descending aorta, carotid artery, abdominal aorta, external ear, femur, skin, liver, spleen, kidney, heart, skeletal muscle, visceral adipose tissue and subcutaneous adipose tissue. One cohort each of P3 and P14 mice was euthanized at six weeks of age and individual tissues collected for DNA-sequencing analysis. Another cohort of P3 and P14 injected mice was euthanized at six months of age and individual tissues collected for DNA, RNA, protein and histological analysis. A separate cohort was followed for longevity. All animal use complied with the Animal Care and Use Committee guidelines under protocol G-03–05 (NIH) and M1800126 (VUMC).

A linear regression of the *t*-distribution of longevity history of the homozygous mice in the colony with mouse sex as a covariate using 12 male or female treated mice versus 12 male or female control mice suggests a significant difference in longevity at 42.0 days with 80% power, or 48.6 days with 90% power. The Mantel–Cox test was used for longevity statistics.

Reporting summary

Further information on research design is available in the Nature Research Reporting Summary linked to this paper.

Data availability

DNA-sequencing files can be accessed at the NCBI SRA with accession code PRJNA627465. Raw data are available in Supplementary Data 1, 2, 3, 5 and 6.

Code availability

Code used in this study is available from https://github.com/CwilsonBroad/Koblan_2020_In-Vivo-Adenine-Base-Editing-Corrects-Hutchinson-Gilford-Progeria-Syndrome (Supplementary Note 3).

48. Doench, J. G. et al. Optimized sgRNA design to maximize activity and minimize off-target effects of CRISPR–Cas9. *Nat. Biotechnol*. **34**, 184–191 (2016).
49. Sanjana, N. E., Shalem, O. & Zhang, F. Improved vectors and genome-wide libraries for CRISPR screening. *Nat. Methods* **11**, 783–784 (2014).
50. Wu, D. & Smyth, G. K. Camera: a competitive gene set test accounting for inter-gene correlation. *Nucleic Acids Res*. **40**, e133 (2012).
51. Cao, K. et al. Rapamycin reverses cellular phenotypes and enhances mutant protein clearance in Hutchinson–Gilford progeria syndrome cells. *Sci. Transl. Med*. **3**, 89ra58 (2011).
52. Ewels, P., Magnusson, M., Lundin, S. & Käller, M. MultiQC: summarize analysis results for multiple tools and samples in a single report. *Bioinformatics* **32**, 3047–3048 (2016).
53. Frengen, E. et al. A modular, positive selection bacterial artificial chromosome vector with multiple cloning sites. *Genomics* **58**, 250–253 (1999).
54. DuBose, A. J. et al. Use of microarray hybrid capture and next-generation sequencing to identify the anatomy of a transgene. *Nucleic Acids Res*. **41**, e70
55. Li, H. & Durbin, R. Fast and accurate short read alignment with Burrows–Wheeler transform. *Bioinformatics* **25**, 1754–1760 (2009).
56. Li, H. et al. The Sequence Alignment/Map format and SAMtools. *Bioinformatics* **25**, 2078–2079 (2009).
57. Quinlan, A. R. & Hall, I. M. BEDTools: a flexible suite of utilities for comparing genomic features. *Bioinformatics* **26**, 841–842 (2010).
58. Tarasov, A., Vilella, A. J., Cuppen, E., Nijman, I. J. & Prins, P. Sambamba: fast processing of NGS alignment formats. *Bioinformatics* **31**, 2032–2034 (2015).
59. McKenna, A. et al. The Genome Analysis Toolkit: a MapReduce framework for analyzing next-generation DNA sequencing data. *Genome Res*. **20**, 1297–1303 (2010).
60. DePristo, M. A. et al. A framework for variation discovery and genotyping using next-generation DNA sequencing data. *Nat. Genet*. **43**, 491–498 (2011).
61. Van der Auwera, G. A. et al. From FastQ data to high confidence variant calls: the Genome Analysis Toolkit best practices pipeline. *Curr. Protoc. Bioinformatics* **43**, 11.10.1–11.10.33 (2013).
62. Wang, K., Li, M. & Hakonarson, H. ANNOVAR: functional annotation of genetic variants from high-throughput sequencing data. *Nucleic Acids Res*. **38**, e164 (2010).
63. Sondka, Z. et al. The COSMIC Cancer Gene Census: describing genetic dysfunction across all human cancers. *Nat. Rev. Cancer* **18**, 696–705 (2018).
64. Buenrostro, J. D., Giresi, P. G., Zaba, L. C., Chang, H. Y. & Greenleaf, W. J. Transposition of native chromatin for fast and sensitive epigenomic profiling of open chromatin, DNA-binding proteins and nucleosome position. *Nat. Methods* **10**, 1213–1218 (2013).

Acknowledgements This work was supported by NIH grants U01AI142756, UG3AI150551, UG3TR002636, RM1HG009490, R01EB022376, R35GM118062, Z01HG200305, R01HL146654 and R01HL126784, and by the Howard Hughes Medical Institute. L.W.K. acknowledges an NSF GRFP fellowship; C.W. acknowledges a Damon Runyon Cancer Research Foundation fellowship (DRG-2343-18); G.A.N. acknowledges a Helen Hay Whitney postdoctoral fellowship; and L.B.G., L.W.K. and D.R.L. acknowledge support from The Progeria Research Foundation.

Author contributions L.W.K., J.D.B., C.Y.L., M.R.E., F.S.C. and D.R.L. designed the research. L.W.K., M.R.E., C.W., W.A.C., L.D., Y.G.G., X.M., G.A.N., S.P.D., J.D.B. performed cell culture experiments. L.W.K., M.R.E., C.W., W.A.C., J.M.L., Z.X., U.L.T., L.D., S.P.D., N.N., Q.S., C.K. and J.D.B. performed in vivo experiments. L.B.G., K.C., F.S.C., J.D.B. and D.R.L. supervised the project. L.W.K. and D.R.L. wrote the manuscript with input from all other authors.

Competing interests D.R.L. is a co-founder of Beam Therapeutics, Prime Medicine, Pairwise Plants and Editas Medicine, companies that use genome editing. The remaining authors declare no competing interests.

Additional information

Supplementary information is available for this paper at https://doi.org/10.1038/s41586-020-03086-7.

Correspondence and requests for materials should be addressed to F.S.C., J.D.B. or D.R.L.

Peer review information *Nature* thanks the anonymous reviewers for their contribution to the peer review of this work.

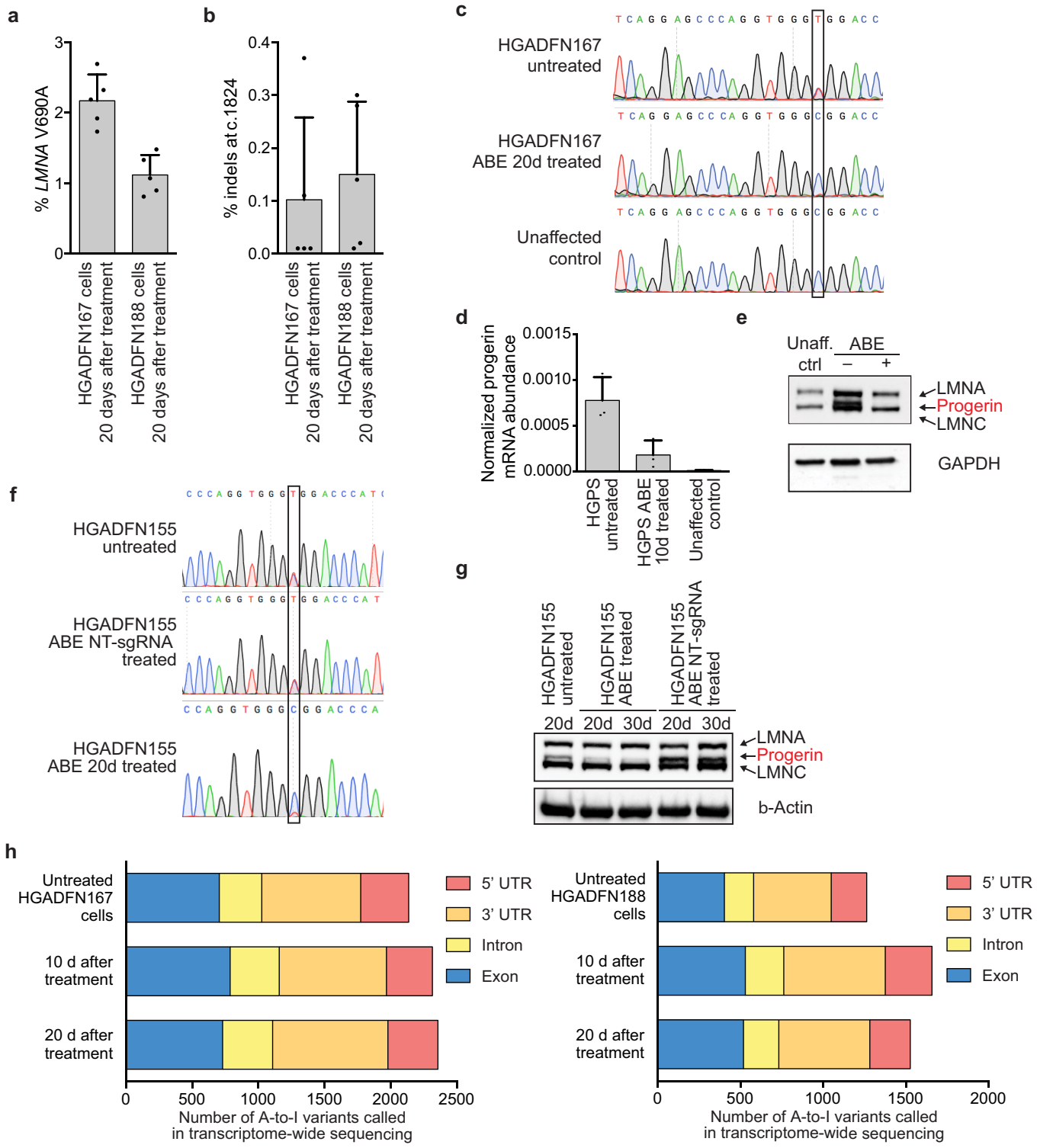

Extended Data Fig. 1 | See next page for caption.

Extended Data Fig. 1 | Additional characterization of patient-derived cells treated with ABE7.10max-VRQR. a, Bystander V690A editing in patient-derived HGADFN167 and HGADFN188 cells 20 days after treatment with lentiviral ABE7.10max-VRQR. **b**, Indel formation frequency at the c.1824 target locus in HGADFN167 and HGADFN188 cells 20 days after treatment with lentiviral ABE7.10max-VRQR. Data are mean ± s.d. for $n = 5$ technical replicates (individual points) for **a**, **b**. **c**, Sanger DNA sequencing traces of untreated HGADFN167 cells, 20-day treated HGADFN167 cells and unaffected control cells. The target nucleotide is boxed. **d**, qPCR-normalized progerin mRNA abundance in cells described in **c**. Data are mean ± s.d. for $n = 3$ biological replicates. **e**, Western blot analysis of HGADFN167 cells described in **c**. LMNA, progerin, and LMNC protein are all stained on the gel, A GAPDH loading control is shown below. An additional replicate is provided in Fig. 1d. Unaff. ctrl, control cells from an unaffected parent. **f**, Sanger DNA sequencing traces of untreated, non-targeting (NT)-sgRNA-treated and ABE-treated HGADFN155 fibroblasts at a 20-day time point to ensure NT-sgRNA did not lead to DNA editing. **g**, Western blot analysis of cells described in **f** as well as treated cells at a 30-day time point. LMNA, progerin, and LMNC proteins are all stained on the gel, a β-actin loading control is shown below. Expected molecular weights: lamin A, 74 kDa; progerin, 69 kDa; lamin C, 65 kDa. Complete blots are available in Supplementary Fig. 1. Additional replication was not performed. **h**, HGADFN167 (left) and HGADFN188 (right) cell lines untreated or treated with lentiviral ABE7.10max-VRQR after 10 or 20 days show similar relative distributions of A-to-I SNVs in their transcriptomes compared with the hg38 human genome reference sequence. On average, 36 ± 3.6% of SNPs in these samples occur with around 100% frequency, suggesting they arise from genomic sequence variations; however, we cannot explicitly exclude them from consideration as no whole-genome sequence is available for these cell lines. Raw counts of 100% edited SNPs per sample are: untreated HGADFN167 cells (849), HGADFN167 10 d after treatment (883), HGADFN167 20 d after treatment (871), untreated HGADFN188 cells (488), HGADFN188 10 d after treatment (501), HGADFN188 20 d after treatment (510).

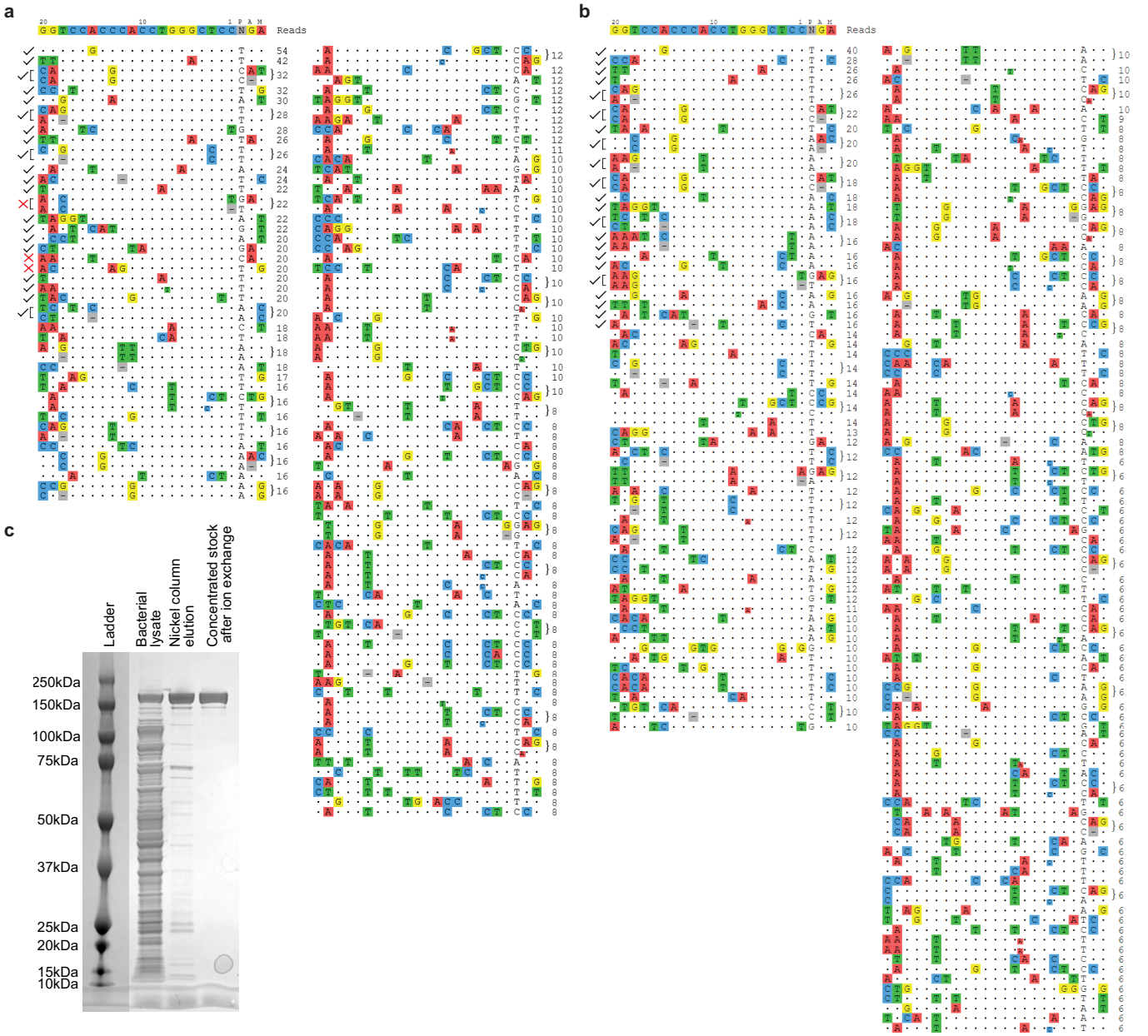

Extended Data Fig. 2 | CIRCLE-seq analysis of HGADFN167 and HGADFN188 cells using Cas9-VRQR and the progeria-targeting sgRNA. a, **b**, CIRCLE-seq read counts for Cas9-VRQR nuclease-treated genomic DNA from HGADFN167 (**a**) and HGADFN188 (**b**) cell lines. Targeted amplicon sequencing was used to assess the off-target base editing for 36 noted total loci distributed across both cell lines. DNA at 32 of 35 loci amplified efficiently from both cell lines (denoted by black check marks), DNA at 3 loci failed to amplify (denoted by red X marks). Complete CIRCLE-seq data are provided in Supplementary Data 4. **c**, SDS–PAGE gel stained with InstantBlue to follow protein purification of Cas9-VRQR. Totals of 0.5 µl clarified lysate, 0.25 µl nickel column elution or 0.1 µl of the concentrated protein stock after His-tag purification and ion-exchange chromatography were added to 5 µl NuPAGE loading buffer. Samples were denatured at 98 °C for 5 min before loading onto the 4–12% acrylamide gel. A Precision Plus Protein Kaleidoscope Pre-Stained Ladder (Bio-Rad) was used as reference. The desired Cas9-VRQR has a predicted molecular weight of 161.9 kDa. Additional replication was not performed.

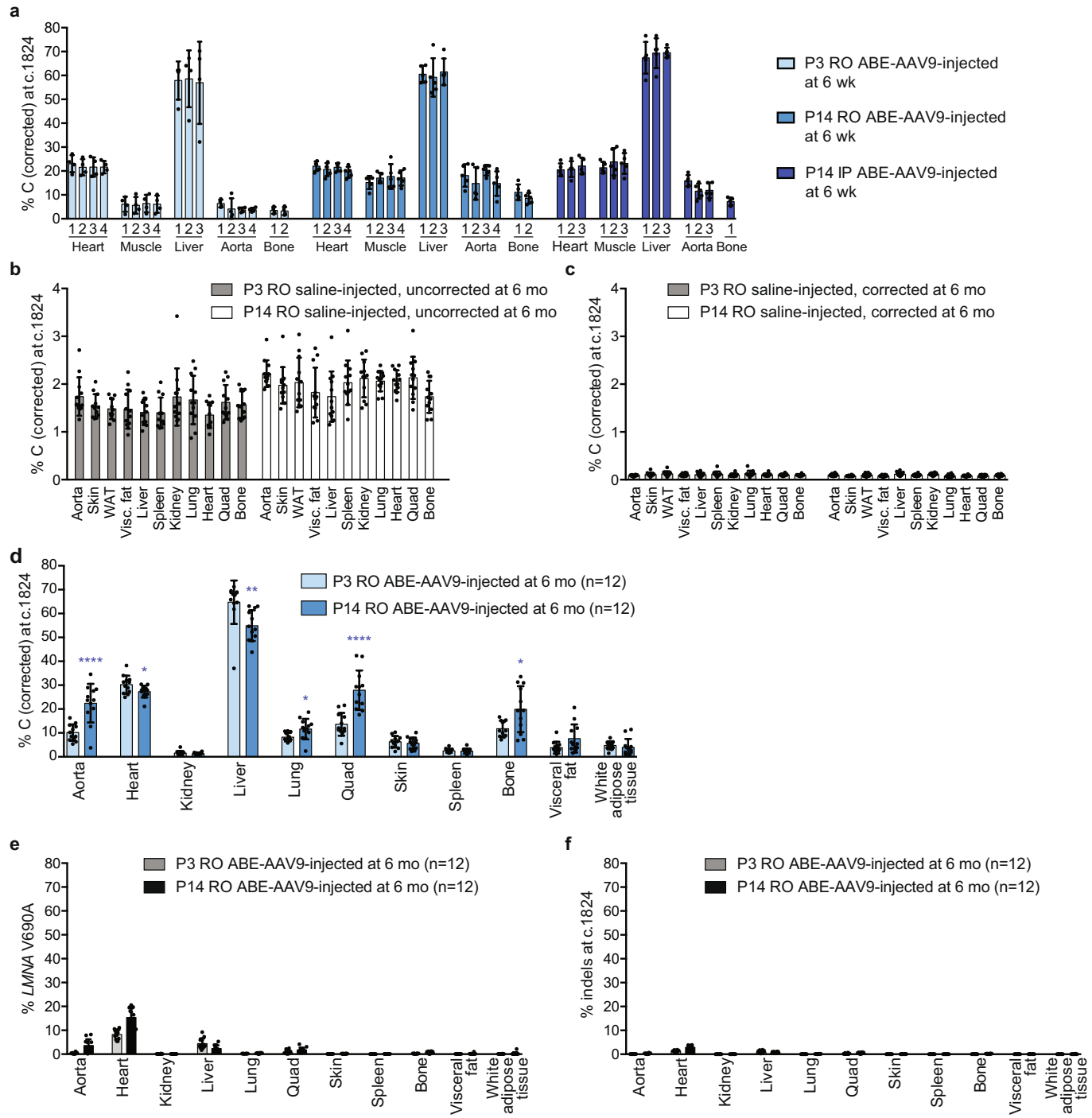

Extended Data Fig. 3 | See next page for caption.

Extended Data Fig. 3 | DNA on-target editing, bystander editing and indel efficiencies across tissues from in vivo injection route optimization experiments. a, Dual AAV9 encoding split-intein ABE7.10max-VRQR base editor halves and the *LMNA*-targeting sgRNA were injected into homozygous *LMNA* c.1824 C>T mice. P3 retro-orbital (RO) injections (5×10^{10} vg of each AAV, 1×10^{11} vg total), P14 RO injections (5×10^{11} vg of each AAV, 1×10^{12} vg total) and P14 intraperitoneal (IP) injections (5×10^{11} vg of each AAV, 1×10^{12} vg total) were tested. At 6-weeks of age, mice were euthanized and heart, muscle, liver, aorta and bone were isolated for sequencing analysis. Tissues were sub-sectioned for sequencing analysis to ensure sub-sections did not show differences in editing efficiencies for downstream analyses. Each bar represents a different tissue subsection. DNA-editing efficiencies correcting *LMNA* c.1824 from T (pathogenic) to C (wild-type) for P3 RO-injected mice (left, $n = 4$), P14 RO-injected mice (middle, $n = 5$) and P14 IP-injected mice (right, $n = 5$) at 6 weeks of age are shown for five disease-relevant tissues. Data are mean ± s.d. **b**, Apparent *LMNA* c.1824 T (pathogenic) to C (wild-type) mutations from tissue samples of saline-injected P3 RO (left) and P14 RO (right) control mice at 6 months of age show background signal due to amplicon crossover during PCR between the human diseased allele and the wild-type mouse allele, which share 90% overall sequence identity within the amplified region. Similar crossover levels were observed across 11 tissues in both P3 RO and P14 RO saline-injected mice. Data are mean ± s.d. for $n = 12$ mice (6 male, 6 female). **c**, Computational filtering of same sequencing reads shown in **b** after removing any reads containing any mouse-specific sequence variations, analysing only reads containing exclusively human sequence. The script used to remove mouse-containing sequencing reads is in the link in Supplementary Note 3 and is described in the Methods ('High-throughput sequencing of in vivo samples'). **d**, DNA editing for P3- and P14-injected mice at 6 months of age across 11 tissues. Each point represents a biological replicate of a tissue taken from a unique mouse ($n = 12$ for each group). **e**, V690A bystander editing frequency across eleven tissues for P3 RO and P14 RO ABE-treated mice at 6 months of age ($n = 12$ for each group). **f**, Indel frequencies at the c.1824 target locus across 11 tissues for P3 RO and P14 RO ABE-treated mice at 6 months of age. Data are mean ± s.d. for the indicated number of biological replicates. $^{*}P < 0.05$, $^{**}P < 0.01$, $^{***}P < 0.001$, $^{****}P < 0.0001$ by Student's unpaired two-sided *t*-test.

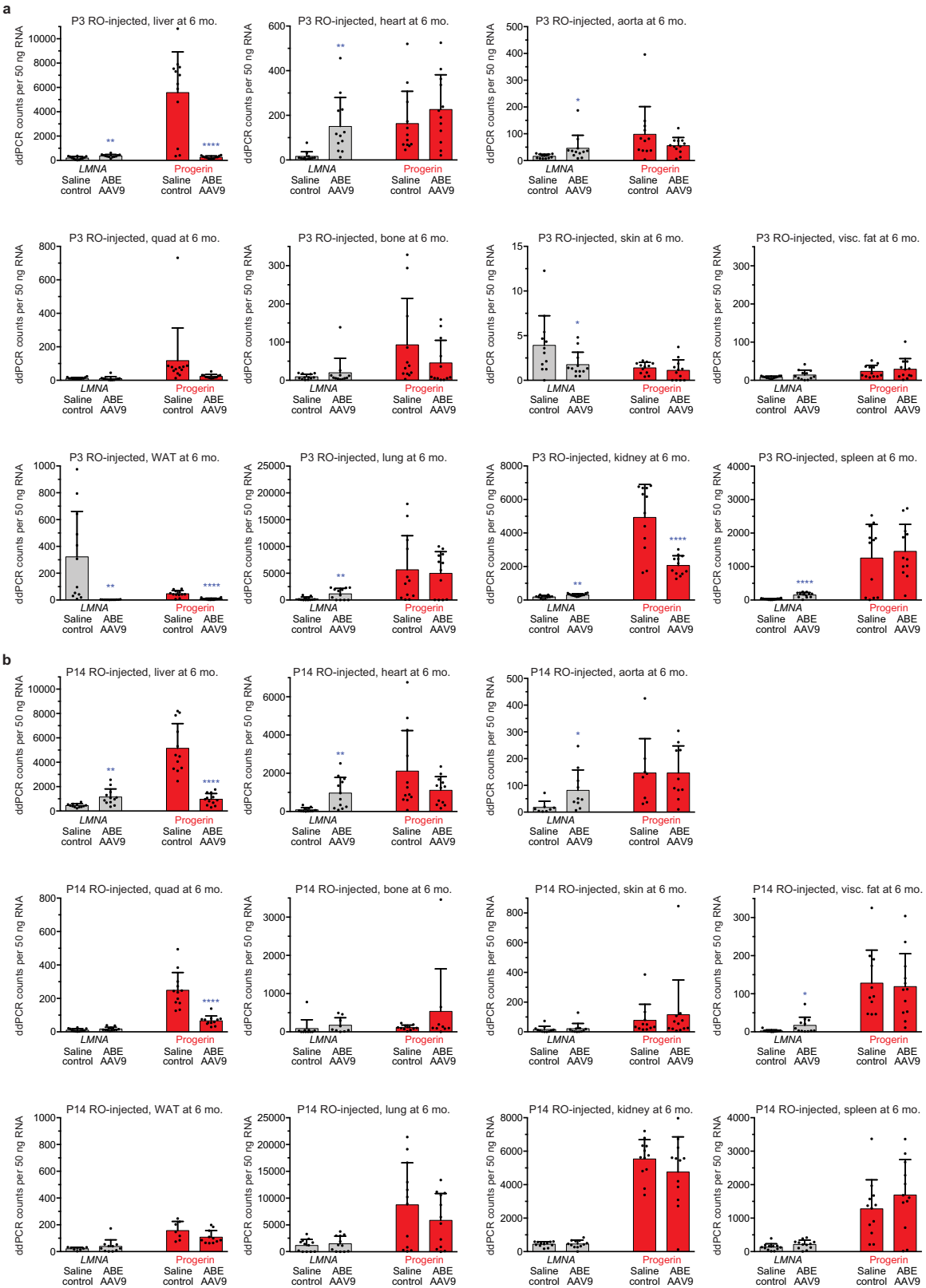

Extended Data Fig. 4 | Quantification of *LMNA* and progerin transcript abundance by ddPCR in mice that were retro-orbitally injected with saline or ABE-AAV9 at P3 or P14. a, ddPCR counts for *LMNA* (grey bars) and progerin (red bars) RNA transcript abundance in P3 RO saline- and ABE-AAV9-injected mice. Data are mean ± s.d. for $n = 12$ mice. **b**, ddPCR counts for *LMNA* (grey bars) and progerin (red bars) RNA transcript abundance in P14 RO saline- and ABE-AAV9-injected mice. Data are mean ± s.d. for $n = 12$ biological replicates for all samples except for saline-injected mouse skin ($n = 11$), WAT ($n = 7$), visceral fat ($n = 11$), tibia ($n = 11$) and aorta ($n = 8$); and ABE-AAV9-injected mouse WAT ($n = 11$), tibia ($n = 9$) and aorta ($n = 10$). Visc. fat, visceral fat. $^{*}P < 0.05$, $^{**}P < 0.01$, $^{***}P < 0.001$, $^{****}P < 0.0001$ by Student's unpaired two-sided *t*-test for **a**, **b**. Liver and heart values are reproduced from Fig. 3c for ease of comparison.

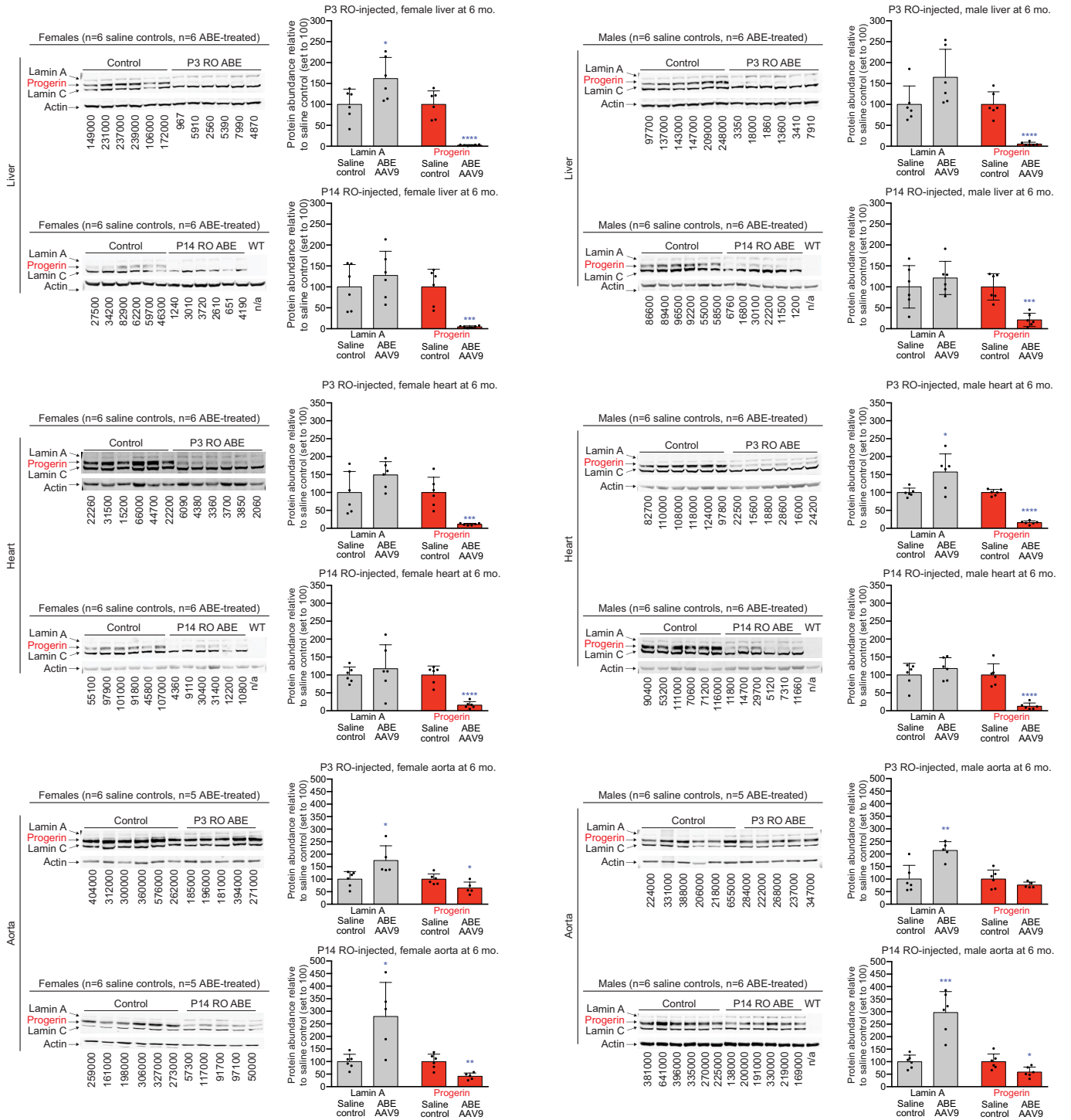

Extended Data Fig. 5 | Quantification of western blots. Liver, heart and aorta tissue western blots for P3-injected (top half of each tissue set) and P14-injected mice (bottom half of each tissue set) were quantified by western blot. Samples from females appear in the left column, and samples from males are in the right column. Each lane represents the tissue type specified on the left taken from a different mouse. Control mice were treated with saline instead of ABE-AAV9. WT indicates C57BL/6 mouse lacking the transgene, showing that the antibody is specific to human lamin proteins and progerin. The abundance of lamin A or progerin protein relative to β-actin in saline- or ABE-treated mouse tissues was quantified by normalizing the fluorescence signal from the secondary antibody for each band (800 nm for progerin and lamins, and 680 nm for actin; see Methods ('Protein isolation and western blotting from mouse tissues'). The normalized protein abundance relative to saline-treated samples (set to 100) is shown in the bar graphs. Control mice were treated identically to the corresponding ABE-treated mice except injected with saline instead of ABE-AAV9. Raw fluorescent signal for progerin protein measured at the 800-nm wavelength (using IRDye-labelled antibody) is displayed under each lane. Data are mean ± s.d. for $n = 5$ or 6 biological replicates, as indicated. The n for each sample type is listed in each figure panel. *$P < 0.05$, **$P < 0.01$, ***$P < 0.001$, ****$P < 0.0001$ by Student's unpaired two-sided t-test. Expected molecular weights: lamin A, 74 kDa; progerin, 69 kDa; lamin C, 65 kDa. Liver and heart blots are reproduced from Fig. 3c for ease of comparison. Complete blots are available in Supplementary Fig. 1.

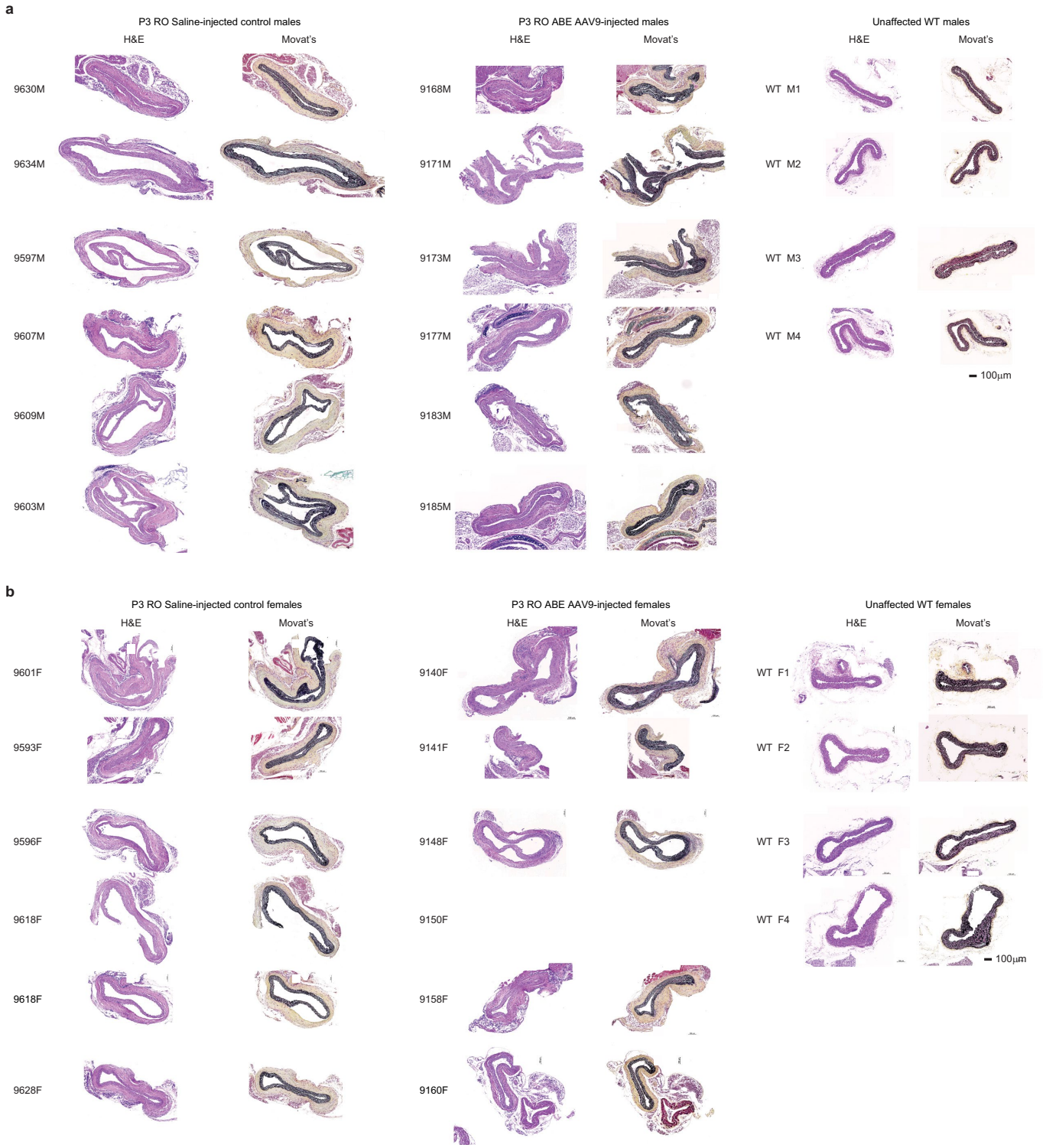

Extended Data Fig. 6 | Aortic histology of male and female mice that were retro-orbitally injected with saline or ABE-AAV9 at P3. a, Representative aorta cross-sections for P3 RO saline- or ABE-AAV9-injected males at 6 months of age. Left images were stained with H&E; right images were stained with Movat's pentachrome stain. **b**, Representative aorta cross-sections for P3 RO saline- or ABE-AAV9-treated females at 6 months of age. Left images were stained with H&E; right images were stained with Movat's pentachrome stain. Unaffected WT are wild-type C57BL/6 mice. WT M2, 9609M, 9177M, WT F3, 9628F and 9148F are reproduced from Fig. 4 for ease of comparison. These sections each represent replicates from different mice.

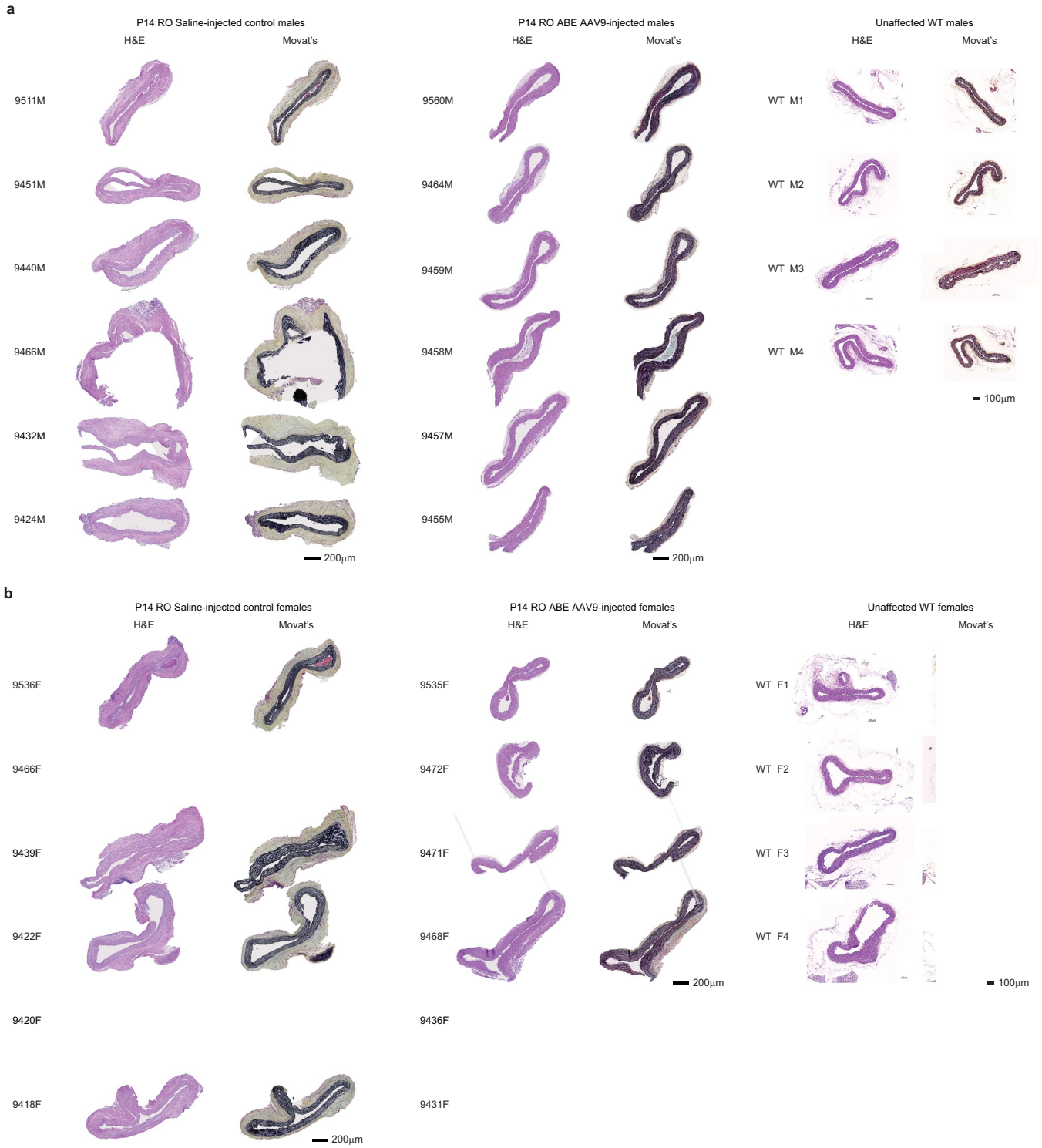

Extended Data Fig. 7 | Aortic histology of male and female mice that were retro-orbitally injected with saline or ABE-AAV9 at P14. a, Representative aorta cross-sections for P14 RO saline- or ABE-AAV9-injected males at 6 months of age. Left images were stained with H&E; right images were stained with Movat's pentachrome stain. **b**, Representative aorta cross-sections for P14 RO saline- or ABE-AAV9-treated females at 6 months of age. Left images were stained with H&E; right images were stained with Movat's pentachrome stain. Unaffected WT are wild-type C57BL/6 mice, reproduced from Extended Data Fig. 9a, b for ease of comparison. Images from the following mice are reproduced from Fig. 4 for ease of comparison: WT M2, 9440M, 9459M, WT F3, 9536F and 9535F. These sections each represent replicates from different mice.

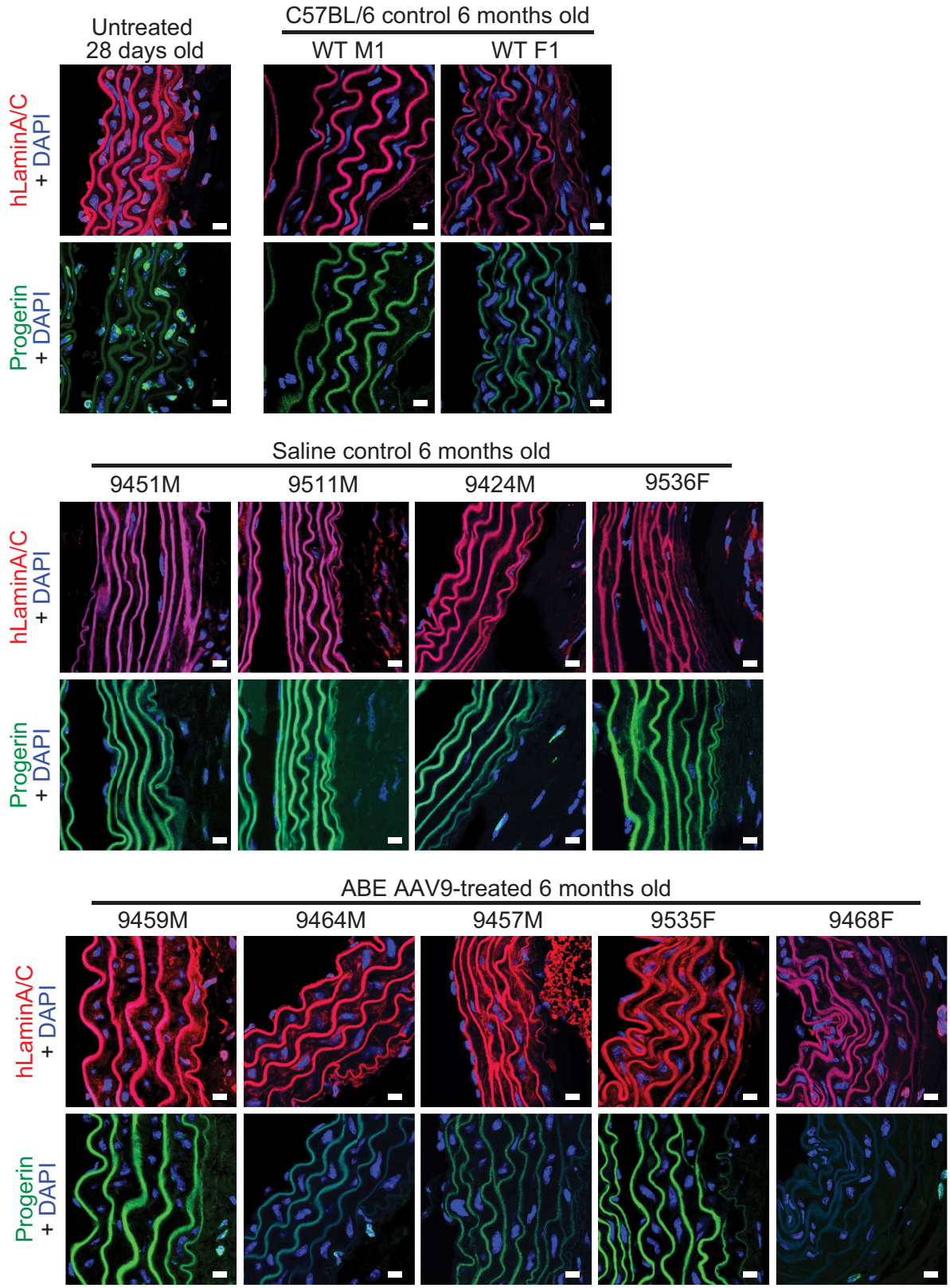

Extended Data Fig. 8 | Immunofluorescence staining of aortas from male and female control C57BL/6 mice, untreated mice and mice that were retro-orbitally injected with saline or ABE-AAV9 at P14. Immunofluorescence staining of C57BL/6 ($n = 2$), untreated P28 homozygous *LMNA* c.1824 C>T ($n = 1$), saline-treated homozygous *LMNA* c.1824 C>T ($n = 4$) and ABE-treated homozygous *LMNA* c.1824 C>T ($n = 5$) mouse aortas stained for human lamin A/C + DAPI or for progerin + DAPI. Scale bars, 10 µm. Images from untreated 28 day-old, WT M1, 9424M and 9464M are replicated from Fig. 4 for ease of comparison.

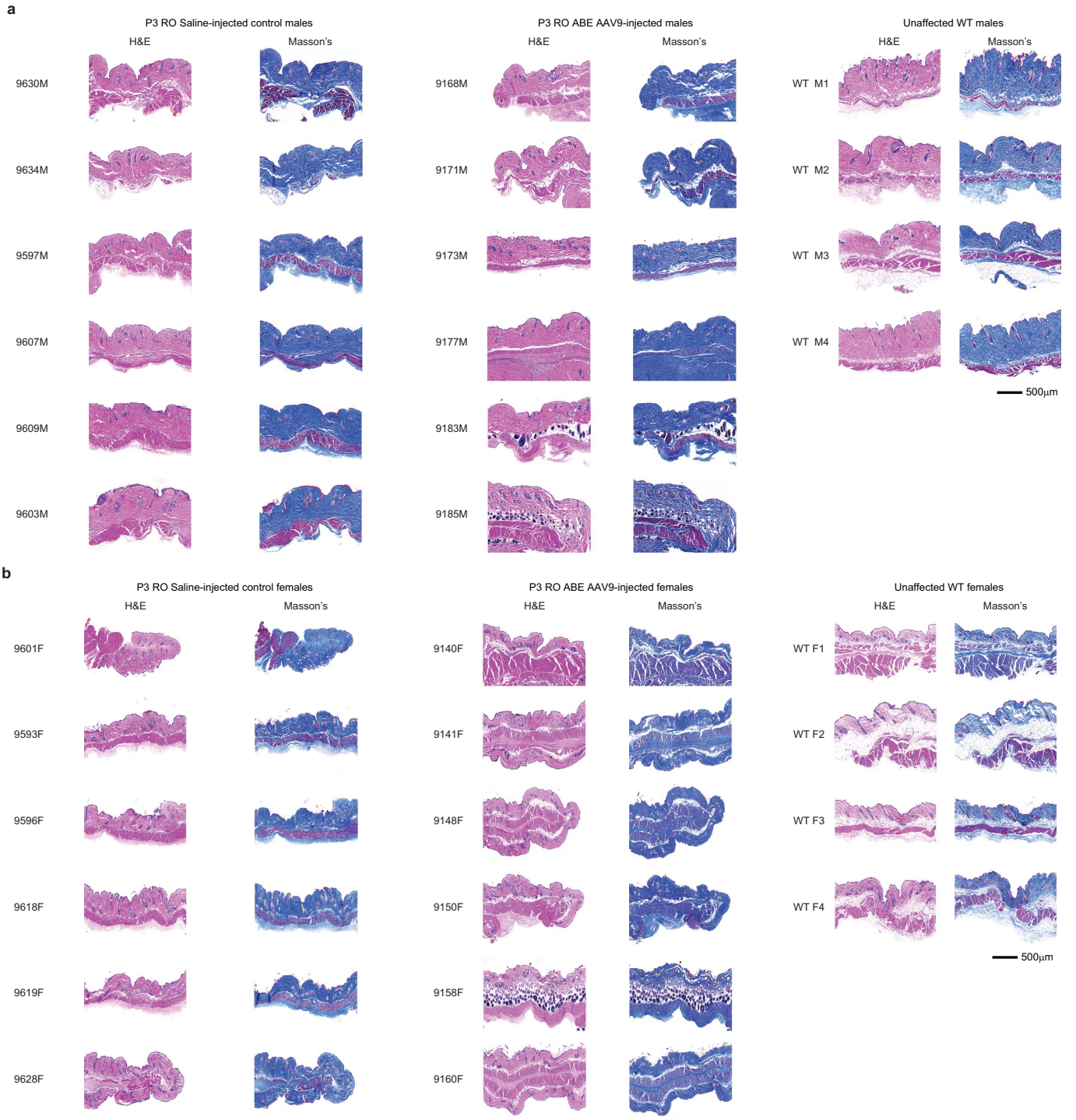

Extended Data Fig. 9 | Skin histology of male and female mice that were retro-orbitally injected with saline or ABE-AAV9 at P3. a, Representative skin cross-sections for P3 RO saline-injected (left), ABE-AAV9-injected (middle) and wild-type C57BL/6 males at 6 months of age. Left images were stained with H&E; right images were prepared with Masson's trichrome staining. **b**, Representative skin cross-sections for P3 RO saline-injected (left), ABE-AAV9-injected (middle) and wild-type C57BL/6 females at 6 months of age. Left images were stained with H&E; right images were prepared with Masson's trichrome staining. Unaffected WT are wild-type C57BL/6 mice. These sections each represent replicates from different mice.

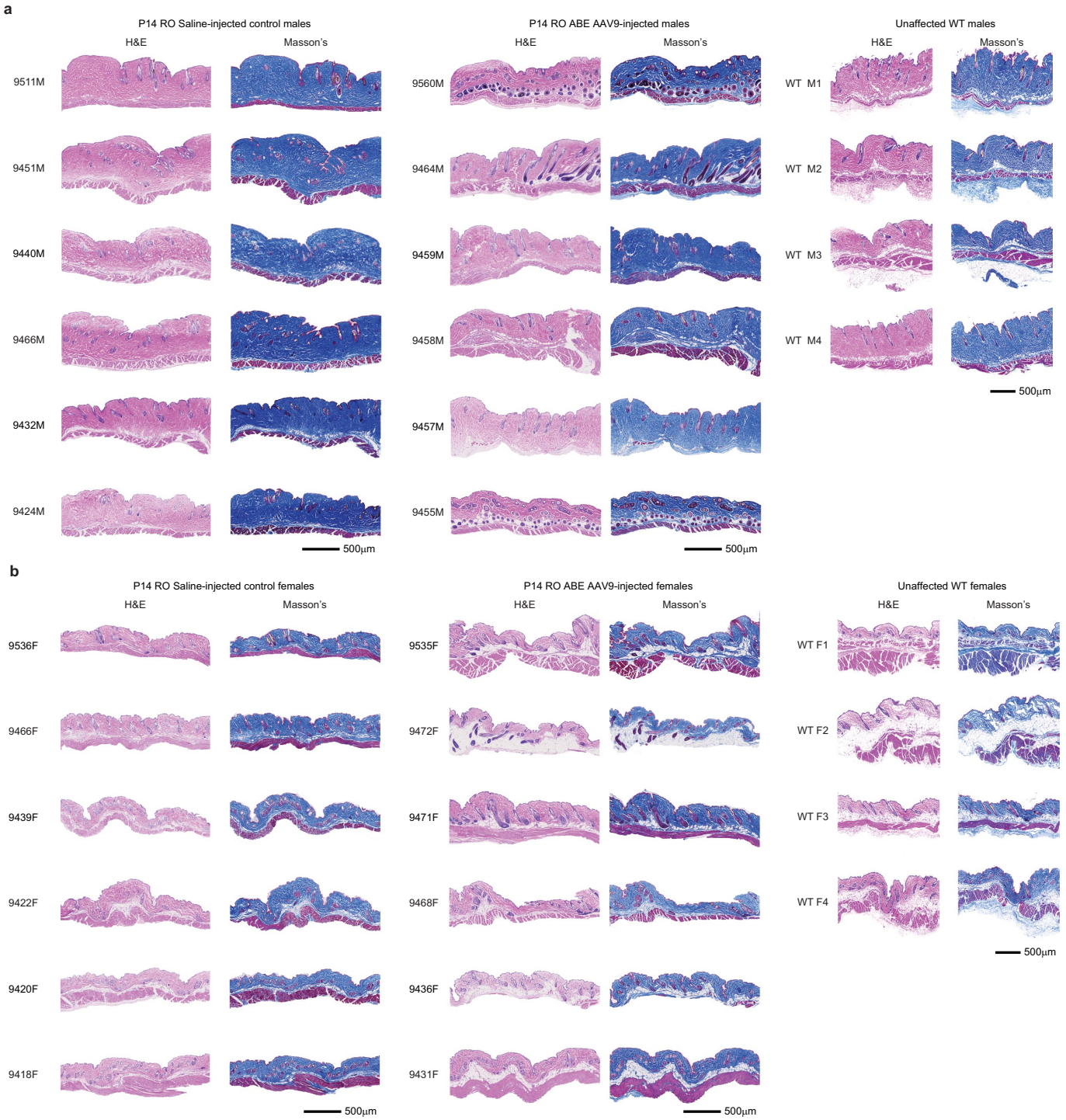

Extended Data Fig. 10 | Skin histology of male and female mice that were retro-orbitally injected with saline or ABE-AAV9 at P14. a, Representative skin cross-sections for P14 RO saline-injected (left), ABE-AAV9-treated (middle) and wild-type C57BL/6 males at 6 months of age. Left images were stained with H&E; right images were prepared with Masson's trichrome staining. **b**, Representative skin cross-sections for P14 RO saline-injected (left), ABE-AAV9-treated (middle) and wild-type C57BL/6 females at 6 months of age. Left images were stained with H&E; right images were prepared with Masson's trichrome staining. Unaffected WT are wild-type C57BL/6 mice, reproduced from Extended Data Fig. 12a, b for ease of comparison. These sections each represent replicates from different mice.

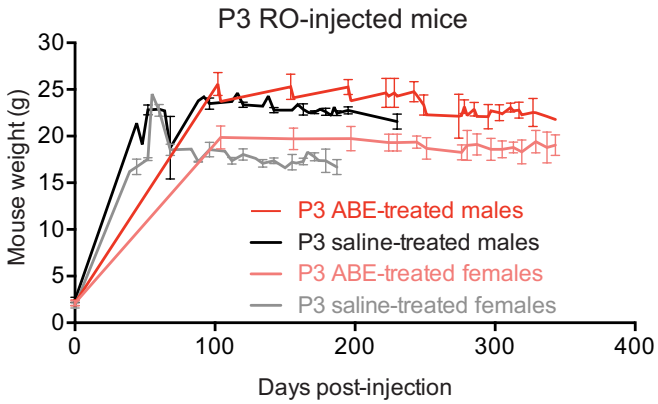

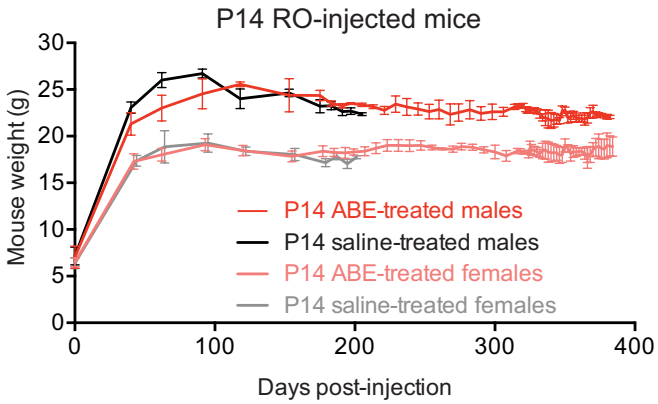

Extended Data Fig. 11 | Body weights of mice that were retro-orbitally injected with saline or ABE-AAV9 at P3 or P14. Weights of homozygous *LMNA* c.1824 C>T mice taken across mouse lifespans for cohorts of P3 RO (left) and P14 RO (right) saline- and ABE-AAV9-injected cohorts. Mouse weights are shown by sex. The *x* axis shows days post-injection, rather than age. Data are mean ± s.d. for the number of surviving mice at each time point; complete data can be accessed in Supplementary Data 5.

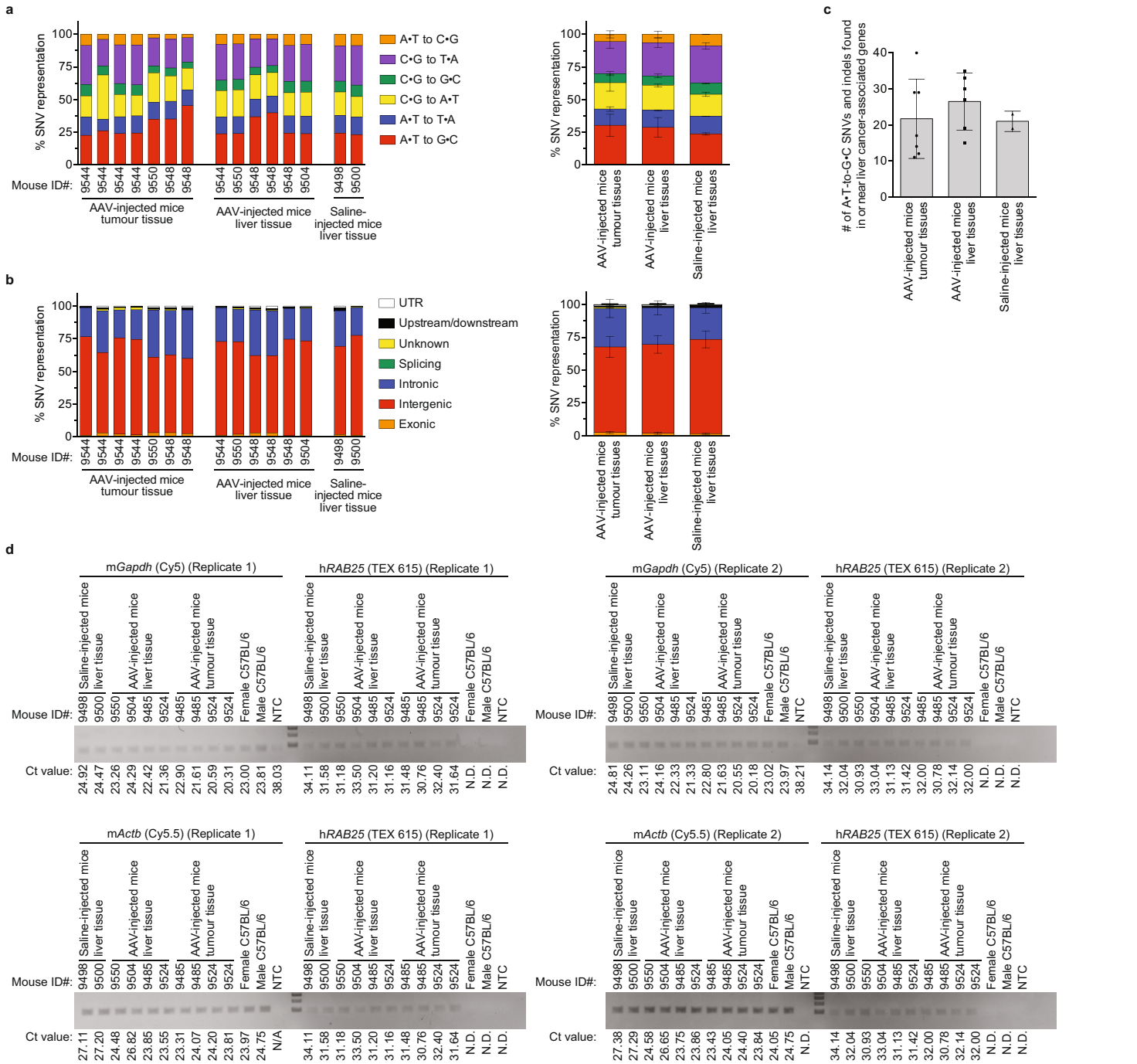

Extended Data Fig. 12 | Whole-genome sequencing analysis of SNVs and indels and quantification of *RAB25* transcript levels in mouse tissue samples. a, Distribution of all possible SNV types in non-tumour liver tissue and liver tumour tissue samples isolated from ABE-AAV9-injected and saline-injected mice. Values from individual tissue samples are shown on the left. Aggregated values from all AAV-injected mouse tumour tissue samples, all AAV-injected mouse liver tissue samples and all saline-injected mouse liver tissue samples are shown on the right. Data are mean ± s.d. with each tissue section treated as a different sample: AAV-injected tumour tissue ($n = 7$), AAV-injected liver tissue ($n = 6$) and saline-injected liver tissue ($n = 2$). **b**, Genomic classification of A•T-to-G•C SNVs. Values from individual tissue samples are shown on the left. Aggregated values from AAV-injected mouse tumour tissue samples, AAV-injected mouse liver tissue samples and saline-injected mouse liver tissue samples from all tissue types are shown on the right. Data are mean ± s.d. with each tissue section treated as a different sample: AAV-injected tumour tissue ($n = 7$), AAV-injected liver tissue ($n = 6$), saline-injected liver tissue ($n = 2$). **c**, A•T-to-G•C SNVs and indels found in or near genes that are recurrently mutated in human liver cancers[63,64] including introns, exons, and at ATAC-seq-defined *cis*-regulatory regions within 100-kb of each gene's transcription start site, in AAV-injected mouse tumour tissue samples, AAV-injected mouse liver tissue samples and saline-injected mouse liver tissue samples. Data are mean ± s.d. Individual data points are shown for each sample. The complete list of SNVs from ANNOVAR analysis is provided as Supplementary Data 6. Summary statistics for SNV calls are in Supplementary Data 2. **d**, RNA isolated from mouse liver tissue samples was reverse-transcribed and amplified with primer sets specific to mouse *Gapdh* (detected with Cy5), mouse *Actb* (detected with Cy5.5) and human *RAB25* (detected with TEX 615). Ct values were determined by quantitative PCR and are shown below each lane. N.D., not detected.

nature research

Corresponding author(s): Francis S. Collins, Jonathan D. Brown, and David R. Liu

Last updated by author(s): Jun 9, 2020

Reporting Summary

Nature Research wishes to improve the reproducibility of the work that we publish. This form provides structure for consistency and transparency in reporting. For further information on Nature Research policies, see Authors & Referees and the Editorial Policy Checklist.

Statistics

For all statistical analyses, confirm that the following items are present in the figure legend, table legend, main text, or Methods section.

n/a	Confirmed	
☐	☒	The exact sample size (*n*) for each experimental group/condition, given as a discrete number and unit of measurement
☐	☒	A statement on whether measurements were taken from distinct samples or whether the same sample was measured repeatedly
☐	☒	The statistical test(s) used AND whether they are one- or two-sided *Only common tests should be described solely by name; describe more complex techniques in the Methods section.*
☒	☐	A description of all covariates tested
☐	☒	A description of any assumptions or corrections, such as tests of normality and adjustment for multiple comparisons
☐	☒	A full description of the statistical parameters including central tendency (e.g. means) or other basic estimates (e.g. regression coefficient) AND variation (e.g. standard deviation) or associated estimates of uncertainty (e.g. confidence intervals)
☐	☒	For null hypothesis testing, the test statistic (e.g. *F*, *t*, *r*) with confidence intervals, effect sizes, degrees of freedom and *P* value noted *Give P values as exact values whenever suitable.*
☐	☒	For Bayesian analysis, information on the choice of priors and Markov chain Monte Carlo settings
☐	☒	For hierarchical and complex designs, identification of the appropriate level for tests and full reporting of outcomes
☒	☐	Estimates of effect sizes (e.g. Cohen's *d*, Pearson's *r*), indicating how they were calculated

Our web collection on statistics for biologists contains articles on many of the points above.

Software and code

Policy information about availability of computer code

Data collection	Illumina Miseq Control software (3.1) was used on the Illumina Miseq sequencers to collect the high-throughput DNA sequencing data. Illumina Nextseq Control software was used on Illumina Nextseq sequencers to collect RNA sequencing data. Illumina Novaseq Control Software (1.7) was used on illumina Novaseq sequencers.
Data analysis	Crispresso2 was used to analyze HTS data for quantifying editing activity at genomic sites. For mouse models a custom Python script was used to preprocesses the HTS data. CIRCLE-Seq data was processed using the CIRCLEseq analysis pipeline (https://github.com/tsailabSJ/circleseq) with parameters: "read_threshold: 4; window_size: 3; mapq_threshold: 50; start_threshold: 1; gap_threshold: 3; mismatch_threshold: 6; merged_analysis: True". RNA-seq alignment: reads where trimmed for quality with TrimGalore version 0.6.2; https://ccb.jhu.edu/software/hisat2/. STAR version 2.7.0d was used to align reads to the version GRCh38(hg38) of the human genome; Differential expression RSEM version 1.3.1 was used to quantify transcript abundance. The limma-voom (3.38.3) and edgeR (3.10) R packages were used to normalize gene expression levels, perform differential expression analysis and visualize results. RNA-seq-AtoI editing: A to I editing was identified using REDItools V2 (https://github.com/BioinfoUNIBA/REDItools) output was analyzed with a R script available. Detailed workflow and custom scripts to be available at https://github.com/CwilsonBroad/Koblan_2020_In-Vivo-Adenine-Base-Editing-Corrects-Hutchinson-Gilford-Progeria-Syndrome. Whole genome Sequencing: We assessed sequence quality of the paired end reads with FastQC (v0.10.0, http://www.bioinformatics.babraham.ac.uk/projects/fastqc/). Alignments where generated with bwa-mem (v0.7.17). Alignment manipulation and extraction was done with samtools (v0.1.18). For SNP calling duplicate reads were removed with Sambamba (https://lomereiter.github.io/sambamba/) variant calling was performed by GATK (https://gatk.broadinstitute.org/hc/en-us) and resulting vcfs where annotated with ANNOVAR (https://annovar.openbioinformatics.org/en/latest/). Zen 2 blue edition, https://www.zeiss.com/microscopy/us/products/microscope-software/zen-lite.html was used for tissue histological analyses. Microsoft Excel for Mac version 16.41 was used for some analysis. Photoshop 21.2.3 was used for some image processing.

For manuscripts utilizing custom algorithms or software that are central to the research but not yet described in published literature, software must be made available to editors/reviewers. We strongly encourage code deposition in a community repository (e.g. GitHub). See the Nature Research guidelines for submitting code & software for further information.

Data

Policy information about availability of data

All manuscripts must include a data availability statement. This statement should provide the following information, where applicable:

- Accession codes, unique identifiers, or web links for publicly available datasets
- A list of figures that have associated raw data
- A description of any restrictions on data availability

High-throughput sequencing data have been deposited in the NCBI Sequence Read Archive database under accession code PRJNA627465.

Field-specific reporting

Please select the one below that is the best fit for your research. If you are not sure, read the appropriate sections before making your selection.

☒ Life sciences ☐ Behavioural & social sciences ☐ Ecological, evolutionary & environmental sciences

For a reference copy of the document with all sections, see nature.com/documents/nr-reporting-summary-flat.pdf

Life sciences study design

All studies must disclose on these points even when the disclosure is negative.

Sample size	Sample sizes were determined based on literature precedence for genome editing experiments (Gaudelli, 2017) (Anzalone, 2019). Sample size was justified by power calculation estimating 90% power to detect differential ages in longevity studies.
Data exclusions	Data exclusions for statistical analysis of mice in Kaplan-Meier curves can be found in text, these mice were determined to have died from causes unrelated to disease and were excluded after observation, exclusion criteria were not pre-established.
Replication	All attempts at replication were successful. Cell line western blots were replicated in Figure 1 and Extended Data Fig. 1. In vivo western blots were not replicated beyond the data presented in the manuscript. Fixed cells were not replicated beyond the data presented. Micrographs were not replicated beyond the reported data.
Randomization	Animals enrolled in both the 6month and longevity studies were randomized while maintaining gender balance.
Blinding	Blinding was not used given that single injections were performed so treatment biases were not possible. Mice were housed, fed, and handled identically. Mice were euthanized according to pre-determined criteria (primary humane endpoint of severe weight loss ≥ 15% in one week, and also included lethargy, failure to thrive, or moribund state as established in approved animal care and use protocol NHGRI G-03-5).

Reporting for specific materials, systems and methods

We require information from authors about some types of materials, experimental systems and methods used in many studies. Here, indicate whether each material, system or method listed is relevant to your study. If you are not sure if a list item applies to your research, read the appropriate section before selecting a response.

Materials & experimental systems

n/a	Involved in the study
☐	☒ Antibodies
☐	☒ Eukaryotic cell lines
☒	☐ Palaeontology
☐	☒ Animals and other organisms
☒	☐ Human research participants
☒	☐ Clinical data

Methods

n/a	Involved in the study
☒	☐ ChIP-seq
☒	☐ Flow cytometry
☒	☐ MRI-based neuroimaging

Antibodies

Antibodies used	Anti-Lamin A + Lamin C antibody [JOL2] (Abcam ab40567) (1:200 for westerns).. Anti-Lamin A/C Antibody, clone 2E8.2, (EMDMillipore MABT538) 1:75 dilution for IF. Anti-progerin antibody (Collins, custom). 1:500 western, 1:300 for cell line IHC, 1:75 for IF. Anti lamin A/C (MAB3211; Millipore). 1:500 for western, 1:250 for cell line IHC. Anti-beta Actin (Abcam #8227, 1:1000) for westerns. H3 Antibody: Cell Signaling Technology, Catalogue # 4499, Lot #9, Rabbit monoclonal. Dilution 1:2000 for westerns. Goat anti-mouse IRdye 800CW, Licor Catalogue # 926-32210, Lot # C90917-25 1:10000 for westerns. Goat anti-rabbit IRdye 680LT, Licor Catalogue # 926-68021; Lot #C90501-06, 1:10000 for westerns. Anti-GAPDH (SC-47724, Santa Cruz) 1:5000 for westerns.

Alexa Fluor 594 donkey anti-rabbit IgG (Invitrogen) 1:1000 for cell line IHC, 1:3000 for IF.
Alexa Fluor 488 donkey anti-mouse IgG (Invitrogen).1:1000 for cell line IHC, 1:3000 for IF.

Validation

• Anti-Lamin A + Lamin C antibody [JOL2] (Abcam ab40567) (1:200 for westerns). (Validation: https://www.abcam.com/lamin-a--lamin-c-antibody-jol2-ab40567.pdf. Validation reference: Varga, et.al.,Proc Natl Acad Sci U S A. 2006 Feb 28;103(9):3250-5. PMID: 16492728.)
• Anti-Lamin A/C Antibody, clone 2E8.2, (EMDMillipore MABT538) 1:75 dilution for IF. Validation: https://www.emdmillipore.com/US/en/product/Anti-Lamin-A-C-Antibody-clone-2E8.2,MM_NF-MABT538#anchor_COA; validation reference: Atchison, et.al., Sci Rep. 2017; 7: 8168.. PMCID: PMC5557922.)
• Anti-progerin antibody (Collins, custom). 1:500 western, 1:300 for cell line IHC, 1:75 for IF. (validation reference: Cao, K. et al. Rapamycin reverses cellular phenotypes and enhances mutant protein clearance in Hutchinson-Gilford progeria syndrome cells. Sci Transl Med 3, 89ra58, doi:10.1126/scitranslmed.3002346 (2011).)
• Anti lamin A/C (MAB3211; Millipore). 1:500 for western, 1:250 for cell line IHC. (Identical to JOL2 antibody; Validation: https://www.abcam.com/lamin-a--lamin-c-antibody-jol2-ab40567.pdf. Validation reference: Varga, et.al.,Proc Natl Acad Sci U S A. 2006 Feb 28;103(9):3250-5. PMID: 16492728.)
• Anti-beta Actin (Abcam #8227, 1:1000) for westerns. (Validation: https://www.abcam.com/beta-actin-antibody-ab8227.html)
• H3 Antibody: Cell Signaling Technology, Catalogue # 4499, Lot #9, Rabbit monoclonal. Dilution 1:2000 for westerns. (Validation : https://www.cellsignal.com/datasheet.jsp?productId=4499&images=1)
• Goat anti-mouse IRdye 800CW, Licor Catalogue # 926-32210, Lot # C90917-25 1:10000 for westerns.
• Goat anti-rabbit IRdye 680LT, Licor Catalogue # 926-68021; Lot #C90501-06, 1:10000 for westerns.
• Anti-GAPDH (SC-47724, Santa Cruz) 1:5000 for westerns. (Validation: https://datasheets.scbt.com/sc-47724.pdf)
• Alexa Fluor 594 donkey anti-rabbit IgG (Invitrogen) 1:1000 for cell line IHC, 1:3000 for IF.
• Alexa Fluor 488 donkey anti-mouse IgG (Invitrogen).1:1000 for cell line IHC, 1:3000 for IF.

Eukaryotic cell lines

Policy information about cell lines

Cell line source(s)

HGADFN167, HGADFN188, HGADFN168 were obtained from the progeria research foundation. HEK293T (ATCC).

Authentication

Cell lines were obtained from the progeria research foundation which catalogues patient-derived cells. Progeria Research Foundation Cell Bank https://www.progeriaresearch.org/cell-and-tissue-bank/
All cell lines are CLIA sequence verified by the Progeria Research Foundation
The PRF Cell and Tissue Bank is Institutional Review Board (IRB) approved by the Rhode Island Hospital Committee on the Protection of Human Subjects, Federal Wide Assurance FWA00001230, study CMTT#0146-09
Cells from ATCC were authenticated by the supplier by STR analysis.

Mycoplasma contamination

All cells tested negative for mycoplasma.

Commonly misidentified lines
(See ICLAC register)

None used.

Animals and other organisms

Policy information about studies involving animals; ARRIVE guidelines recommended for reporting animal research

Laboratory animals

C57BL/6-Tg(LMNA*G608G)HClns/J Stock No: 010667 https://www.jax.org/strain/010667
C57BL/6J Stock No: 000664 https://www.jax.org/strain/000664

Ages incorporated in longevity study from 3 days to >550days, equivalent numbers of male/female.
Animals were housed 1-6 individuals same sex, same strain per cage. Temperatures were maintained 18-230C with humidity 24-60% on 12 hour light/dark cycle.

Wild animals

The study did not involve wild animals.

Field-collected samples

The study did not involve samples collected from the field.

Ethics oversight

The Broad IACUC provided ethical guidance and NIH/NHGRI ACUC protocol NHGRI G-03-5 and M1800126 (VUMC). Mice were housed in barrier facilities with a 12-h light/dark cycle at both National Institutes of Health (NIH) and Vanderbilt University Medical Center (VUMC). Genotyping was performed using standard PCR methods with primers: TTGGACCAAACAAGTACATATCA (Common Forward); CCAATGATAGTGACAGGTATACGG (Wild Type Reverse); CTGACATTCTAGTGGAGGGAGA (Mutant Reverse). Body weights were measured and recorded during health observation twice per week. Mice were injected with split AAV constructs at postnatal day 3 (P3, retro-orbital, 1011 viral genomes total in 10 microliter total volume) or postnatal day 14 (P14, retro-orbital and intraperitoneal, 1012 viral genomes total in 100 microliter total volume). All retro-orbital injections were performed at NIH, while intraperitoneal injections were done at VUMC. Full pathological examination included the ascending aorta, descending aorta, carotid artery, abdominal aorta, external ear, femur, skin, liver, spleen, kidney, heart, skeletal muscle, visceral adipose tissue and subcutaneous adipose tissue. One cohort of P3 and P14 animals were euthanized at 6 weeks of age and individual tissues harvested for DNA sequencing analysis. Another cohort of P3 and P14 injected mice were euthanized at 6 months of age and individual tissues harvested for DNA, RNA, protein and histological analysis. A separate cohort was followed for longevity. All animal use complied with the Animal Care and Use Committee guidelines under protocol G-03–05 (NIH) and M1800126 (VUMC).

Note that full information on the approval of the study protocol must also be provided in the manuscript.